An Automatic Diagnosis of Lung Diseases by Analyzing an Inhomogeneous Motion on 3D shape of lung CT images

Pikul Vejjanugraha

Japan Advanced Institute of Science and Technology

Doctoral Dissertation

An Automatic Diagnosis of Lung Diseases by Analyzing an Inhomogeneous Motion on 3D shape of lung CT images

Pikul Vejjanugraha

Supervisor: Professor Kazunori Kotani

School of Information Science

Japan Advanced Institute of Science and Technology

September 2020

Abstract

This research introduces the new approach of the 3D active contour model to evaluate the velocity vectors of the lung motion and learning the inhomogeneous motion pattern from each lung lobe to generate the predictive model. The non-rigid registration model by using its biophysical model is applied. The velocity vectors between EI and EE models are evaluated by the corresponding points on the parametric surface model of the EE model to the EI model. The external energy from the EI models is the external force that pushes the 3D parametric surface reaching the boundary. The external forces such as balloon force and Gradient Vector Flow (GVF) were adjusted adaptively based on the Z_{ratio} which calculated from the ratio of the maximum value of EI to EE model in Z axis. Next, the feature representation is studied and evaluated based on the lung structure which is separated into 5 lobes. The hierarchical classification is applied to screen the lung diseases into normal, obstructive lung, and restrictive lung by using the stepwise regression and Artificial Neural Network techniques. Lastly, the inhomogeneous motion pattern of lungs integrated with the medical based knowledge can be used to analyze the lung diseases: firstly, by differentiating normal and inhomogeneous motion pattern, secondly by separating restrictive and obstructive lung diseases and thirdly basing on the cause and location of the disease which is the function of the immune and lymphatic system.

Keywords: *3D Active Contour Model, non-rigid registration, inhomogeneous motion pattern, velocity vector map, hierarchical classification*

Acknowledgements

Foremost, I would like to express my great appreciation and sincere gratitude to my supervisor, Prof. Kazunori Kotani, for the continuous support with constructive and valuable suggestions since the beginning throughout many years of research experiences. His willingness to give his time for ongoing guidance has been very much appreciated.

I would like to express my truthful thanks to my co-advisors Prof. Hiroyuki Iida for their valuable advices and useful critiques of this research. Also, I would like to thank committee's members, Prof. Mineo Kaneko, Prof. Jianwu Dang, Assoc. Prof. Shinobu Hasekawa, Assoc. Prof. Waree Kongprawechnon, and Assoc. Prof. Toshiaki Kondo for their support, emparty, and useful suggestion.

A very special thanks to the SIIT-JAIST-NECTEC Dual Doctoral Degree Scholarship Program at Sirindhorn International Institute of Technology (SIIT), Thammasat University, Thailand and Japan Advanced Institute of Science and Technology (JAIST), Japan, for giving me an opportunity for Ph.D. study in Japan. Finally, I would like to thank my family and my friends for their support and encouragement throughout my study.

Contents

List of Figures

List of Tables

Chapter 1

Introduction

1.1 Background

A lung is a vital and heterogeneous organ in the human body. An abnormality of respiration leads to regional differences, depending on diverse functions in the lymphatic system, immune system, metabolic system, and also on mechanical properties such as the gravity force. According to the World Health Organization (WHO) [1], lung diseases, especially Chronic Obstructive Pulmonary Disease (COPD), are the third leading cause of deaths globally in 2016. It was found that the death rate from impaired lungs is increased by the primary risk factors, which are tobacco use, air pollution, chemicals, viruses, and bacteria. The lower respiratory infection and trachea, bronchus, and lung cancer also includes in the top 10 global causes of death. The cause factors directly affect our daily life nowadays. The early detection of respiratory abnormality is essential to consider when it is reversible or almost fully reversible. The predominant diseases in each regional lobe can be divided into three regions: upper lobe, middle lobe, and lower lobe. Disease characterization is challenging because of its diversity in many aspects. It can be considered by lung components such as airways, air sacs, interstitium, blood vessels, pleura, and chest wall. Initially to diagnose a lung disease is to distinguish an obstructive lung disease and a restrictive lung disease. In the physical level, a patient who has obstructive lung disease has difficulty during expiration because of the narrowed or blocked airways (airflow limitation). The remaining air inside affects the residual volume (remaining high) of the lung and leads to the air trapping and hyperinflation problems which can be observed in the anterior-posterior (AP) axis of CT images. In contrast, a restrictive lung disease limits the ability to inhale air. The patient cannot take a deep breath, which affects the total lung capacity and residual volume (low).

The criteria to diagnose obstructive and restrictive lung diseases is defined by the Pulmonary Function Tests (PFTs). The PFTs consist of three main parameters: 1). The Forced Vital Capacity (FVC) test shows the amount of air that a person can quickly and forcefully breathe out, after a deep breath, 2). The Forced Expiratory Volume in One Second (FEV1) test shows the amount of air a person can forcefully exhale in one second of the FVC test, and 3). The Total Lung Capacity (TLC) test describes the volume of air remaining in the lung after exhalation. The FEV_1/FVC ratio is used to diagnose the type of lung disease and the severity of a disease. The FEV_1/FVC ratio is decreased in the obstructive pattern and increased in the restrictive pattern. For example, an FEV_1/FVC ratio of less than 0.7 [19] is considered as COPD and the stage of COPD is classified by the percent of FEV_1: Mild $FEV_1 \geq 80\%$, Moderate $50\% \leq FEV_1 < 80\%$, Severe $30\% \leq FEV_1 < 50\%$, and Very Severe $FEV_1 < 30\%$. These tests are the gold standard to diagnose COPD. The TLC is increased or normal in an obstructive pattern by the remaining air in the lungs and decreased in a restrictive pattern. These characteristics of lung patterns are detected and analyzed to diagnose lung diseases. However, to identify a complex lung disease, thorough lung function testing is required, such as an X-ray, CT-scan. In this work, the Deep Inspiration Breath-Hold (DIBH) technique of CT-scan is used to characterize two different phases of respiration which are the End Inspiratory Phase (EI-images) and End Expiratory Phase (EE-images).

Nowadays, there are some difficulties for radiologists to analyze the two images (EI and EE images) at one time. They need to separately examine EI and EE images on two monitors and manually locate anatomical reference points between the two models, such as blood vessels, spinal cord (Thoracic Vertebrae), and trachea, to diagnose diseases. This requires experience to detect the abnormalities for answering the clinical questions on a diagnostic test. Therefore, to interpret the medical information from the two phases of respiratory CT images (EI and EE images) is still a research gap at present.

This research introduces a new approach to determine the velocity vector map of the lungs from paired inspiratory-expiratory chest CT images from the 3D Active Contour Model (3D ACM) technique. 3D ACMs are frequently used in medical image analysis because they

can detect a non-rigid object by using the parametric curve and the parametric curve drives by the potential forces from the boundary of the target object. In this work, the ACM is used to overcome the non-rigid registration of the deformation surface, and its external force is also useful to help in estimating the expanding motion of the lung. The computing time can also be reduced by using the ACM.

1.1.1 Lung diseases

- Restrictive lung disease has the limited expansion of the lungs in the inspiration. The lung becomes smaller in volume and the patient has to work harder to breathe against the decreased compliance which relates to the PFTs in the decreased total lung capacity (TLC). There are also many types of restrictive lung diseases such as Idiopathic Pulmonary Fibrosis (IPF), Usual Interstitial Pneumonia (UIP), Tuberculosis (TB), Pulmonary fibrosis, Pneumonia. Each disease may have a different course of disease but it shows the same restrictive pattern of the respiratory function.

- Obstructive lung disease is about the narrowed airway leading to increased resistance to airflow during expiration. The airways are mostly concerned with obstructive lung disease. It may have the air-trapping problem because of the narrowed airway and it happens when the patient has difficulty exhaling. When testing with the PFTs, it also shows that the airway flow rates are decreased. When the respiratory function is not well functioned, the ability to expand and shrink is dropped as shown in Fig. 1.1 compared to Fig 1.2.

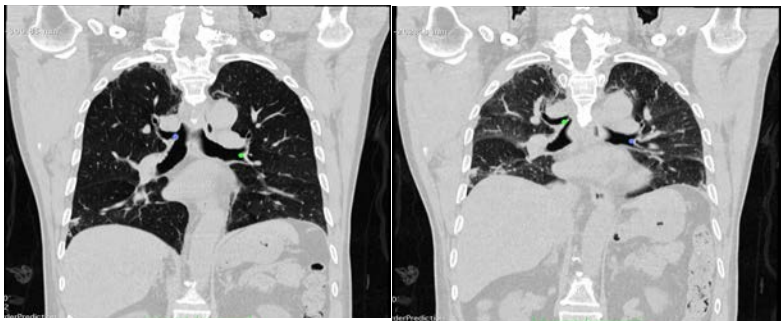

Fig. 1.1. Show the example of respiratory function: (Left) inspiratory, (Right) expiratory.

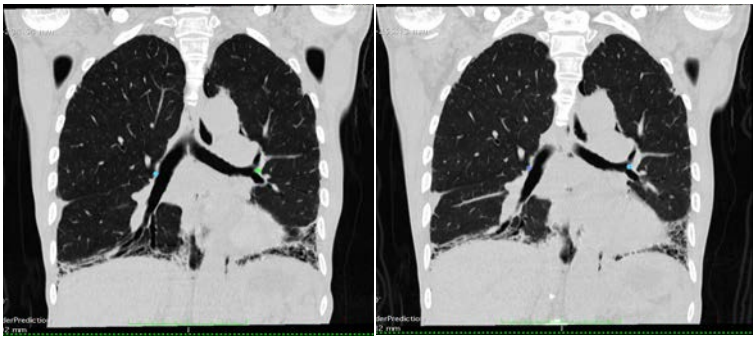

Fig. 1.2. Show the example of respiratory function and its disability to expanding and shrinking: (Left) inspiratory, (Right) expiratory.

The inhomogeneous expanding motion of the lung can be used to analyze lung disease especially the expanding of the lower lobe to the inferior and the expanding of upper lobe to the anterior. Table 1.1 compares the restrictive and obstructive lung disease in different viewpoints and because of the reasons explained in Table 1.1, it affects the inhomogeneous expanding motion pattern of the lung as shown in Fig. 1.1 and Fig. 1.2.

In Fig. 1.2, the expiration (right) has almost the same height (vertical direction) as the inspiratory (left). This motion pattern is collected to the learning machine process to analyze and predict the type of lung diseases based on their characteristic moving pattern.

Table 1.1 The difference between obstructive and restrictive lung disease.

Obstructive Lung Disease	**Restrictive Lung disease**
Characterized by: Air flow Decreased airway flow rates	Characterized by: Lung volume Decreased lung volumes or capacities
Considered: FEV1, FEV1/FVC	Considered: TLV<80%
Anatomy affected: airways	Anatomy affected: lung tissue or thorax
Breathing difficulty: expiration	Breathing difficulty: Inspiration
Pathophysiology: Increased airway resistance	Pathophysiology: Reduced lung or thoracic compliance

1.1.2 Clinical Procedures

- Pulmonary function tests (PFTs)

Pulmonary function tests used a spirometer to measure the ability to breath.

The FVC (Forced Vital Capacity) shows the amount of air that a person can breathe out, quickly and forcefully, after a deep breath. The FEV_1 (the Forced Expiratory Volume in One Second) shows the amount of air a person can forcefully exhale in one second of the FVC test. The ratio of FVC and FEV_1 can help the medical doctors diagnose the specific type of lung disease and the severity of their condition. In addition. PFTs can determine obstructive or restrictive lung diseases. In the **obstructive lung disease** airways are narrowed, which result in resistance to airflow during breathing. The signal to detect the abnormality in obstructive disease or decreased expiratory flow rate or FEV_1. Examples of obstructive lung diseases are asthma, COPD, bronchiectasis, cystic fibrosis, and bronchiolitis. In **restrictive lung disease**, expansion of the lung is limited by disease that affects the chest wall, pleura, or lung tissue itself. The abnormal signal of restrictive lung disease is decreased total lung capacity (TLC). TLC is the volume of air in the lungs after a maximum inspiration. The examples of lung conditions that stiffen and scar the lung are pulmonary fibrosis, radiation damage to the lung, and pneumoconiosis. However, the PFTs still have some limitations to understand the lung tissue pattern and also the details about physiology of each lobe. Fig 1.3 shows the result of PFTs by different types of lung disease such as normal, early small airways obstruction, chronic obstructive disease, fixed large airway obstruction, variable extra thoracic large airway obstruction, and restrictive disease. It shows the ability to breath by flow (L/sec) and also the volume of the lung (%FVC).

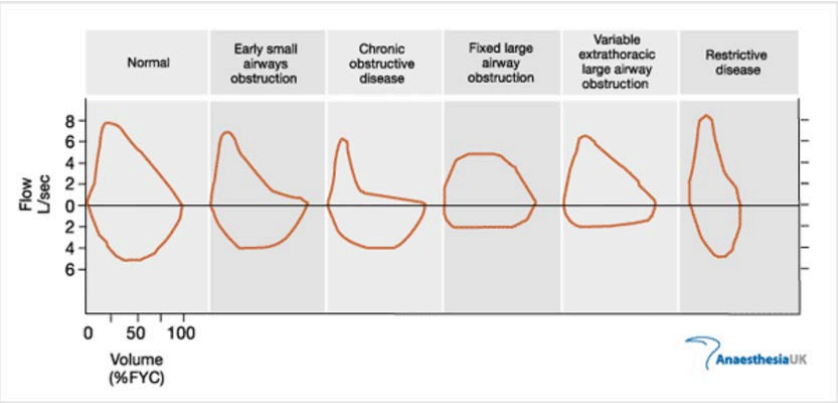

Source: CTS Position Statement: Pulmonary physiology laboratory personnel qualifications. California Thoracic Society, 1998.

Fig. 1.3. The result of PFTs with different specific type of lung diseases.

- Chest X-ray

The imaging procedure uses a small amount of radiation. It can be used to indicate a large variety of chest diseases such as emphysema, pneumonia, cancer, cystic fibrosis, etc. It is quick and fast for the first screening. However, there are some limitations of using 2D X-ray images to analyze the complex or overlapped lung diseases. The occlusion problem and detection error from unclear information may appear. Even the X-ray image can be taking in the frontal (coronal) plane as posteroanterior (PA) or anteroposterior (AP) views and in the sagittal plane as lateral views but it is still not enough to analyze or to make the medical decision in suspect fracture case. It is possible that small masses cannot be detected in the regular film. However, medical doctors often used X-ray as a first screening technique to rule out obvious things before an advanced modality is applied such as CT-scan or MRI-scan.

- Computed Tomography (CT) scan

The multiple views with the different angles are needed to clarify to confirm the disease. This test is for diagnosis of lesions difficult to access by conventional x-ray images such as lung tissue, mediastinum, and pleura. The breath-hold technique is used for the CT-images by taking two shots: end inspiratory (EI) and end expiratory (EE). EI is the moment when the patient holds the full inhalation, and the EE is when the patient holds at the end of expiration as shown in Fig. 1.4. The comparison of PFTs, X-ray, and CT-scan protocols is shown in Fig. 1.5.

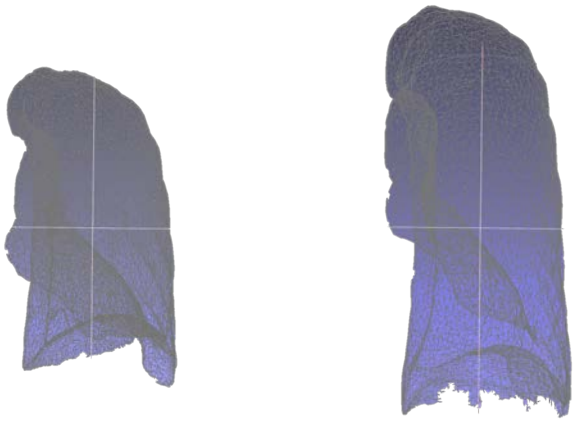

Fig.1.4. 3D model of lungs: (left) End Expiratory (EE) and (right) End Inspiratory (EI).

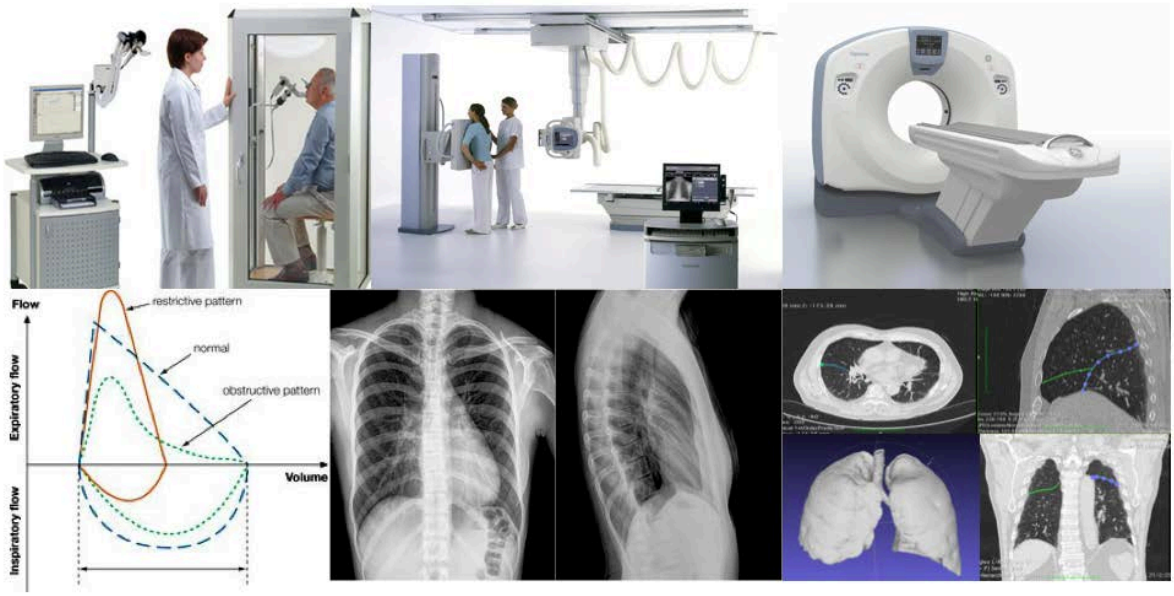

Fig. 1.5. The PFTs, X-ray, and CT-scan and their examination results.

1.1.3 Anatomy of lung

The anatomy and structure of the lung which is described in this section is considered on the important information for understanding the medical terms and also the function of each part. The respiratory function for gas exchanging consists of three important parts: trachea, bronchi, and alveoli as shown in Fig. 1.6. the trachea is the main airway to flow the air into the lung and then it will pass through a smaller air tube called bronchi separated into two main

bronchi for left and right lung and several lobar bronchi for each lung lobe. Finally, the air will reach the end called alveolar sacs which are the exchanging gas organ.

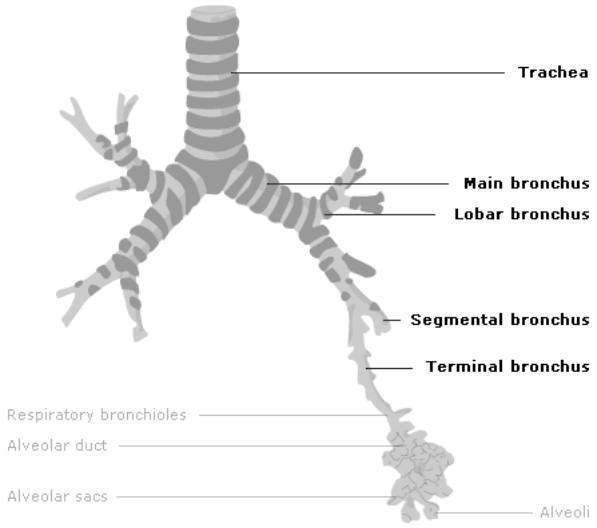

Figure 1.6 Trachea, bronchi, and alveoli.

The structure of the lungs, not only the trachea, bronchi, and alveoli, also included the oblique fissures and horizontal oblique fissure as shown in Fig. 1.7 and Fig. 1.8 for left and right lungs. The oblique fissures also called major fissures appear in both left and right lungs but the horizontal oblique fissure only appears in the right lung. Normally the angle of the oblique fissure is approximately 45 degrees with respect to the z-axis and the angle of the horizontal oblique fissure is almost parallel to the XY-plane or 90 degrees with respect to the Z-axis. As mentioned in [24], they observed the pattern of the oblique fissures and horizontal oblique fissures and it was found that the horizontal fissure is horizontal oriented. When there is the presence of disease which either pushes or pulls the fissure, the horizontal fissure will be displaced as shown in Fig. 1.9

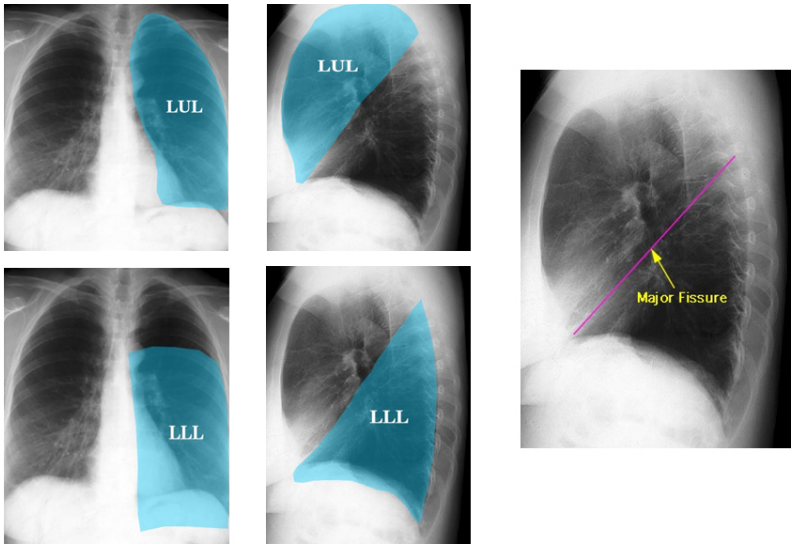

Fig. 1.7. The left lung with two lobes and one fissure [24].

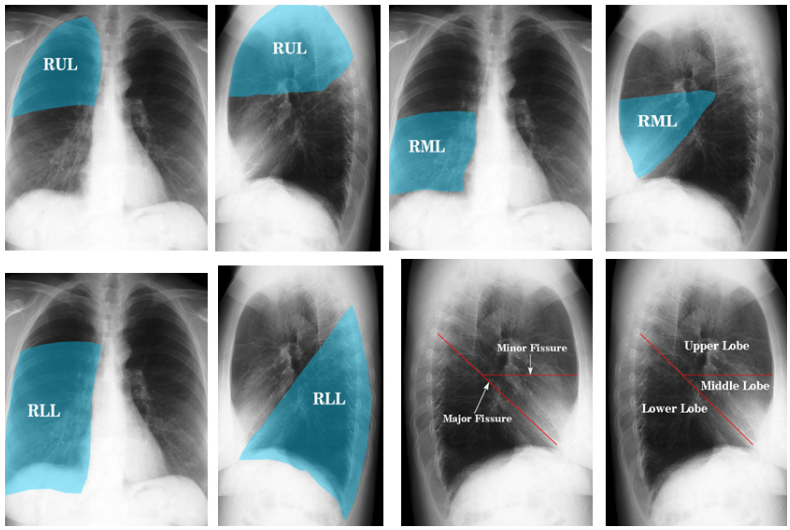

Figure 1.8: The right lungs with three lobes and two fissures [24].

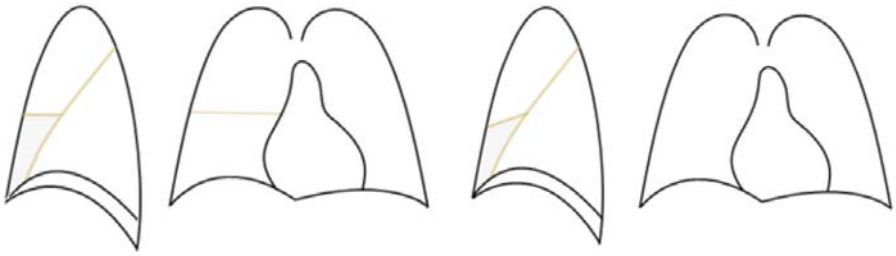

Fig. 1.9. Horizontal oblique fissure: (left) horizontally oriented, (right) displaced inferiorly in case of RML collapse. [24]

1.1.4 Research story

This research introduces the new approach of the 3D active contour model to evaluate the velocity vectors of the lung motion and learning the inhomogeneous motion pattern from each lung lobe to generate the predictive model. The non-rigid registration model by using its biophysical model is applied. The velocity vectors between EI and EE models are evaluated by the corresponding points on the parametric surface model of the EE model to the EI model. The external energy from the EI models is the external force that pushes the 3D parametric surface reaching the boundary. The external forces such as balloon force and Gradient Vector Flow (GVF) were adjusted adaptively based on the Z_{ratio} which calculated from the ratio of the maximum value of EI to EE model in Z axis. Next, the feature representation is studied and evaluated based on the lung structure which is separated into 5 lobes. To screening the lung diseases into normal, obstructive lung, and restrictive lung, the stepwise regression and Artificial Neural Network technique are used to evaluate the result. In conclusion, the inhomogeneous motion pattern of lungs integrated with the medical based knowledge can be used to analyze the lung diseases: firstly, by differentiating normal and inhomogeneous motion patterns, secondly by separating restrictive and obstructive lung diseases and thirdly basing on the cause and location of the disease which is the function of the immune and lymphatic system.

1.2 Motivation and Problem Statements

1.2.1 Motivation

The prior motivation comes from my interest in Biomedical Image Processing. Normally, the research trends are the image segmentation and pattern recognition. The motion pattern of the lung while breathing is very interesting to analyze. The motion pattern of inhomogeneous motion of non-rigid objects is the main scope of this research. To detect the motion of the lung which does not need the manually registration points is considered. Therefore, 3D Active Contour Model is selected by using its parametric surface as the predictive surface of the motion from the EE to EI model. Moreover, the next research question is shifted to which part of the lung that is important to analysis. Therefore, the velocity vector map of the

lung model is divided into five lung lobes to feed in the machine learning module to screening the type of lung diseases.

1.2.2 Problem statements

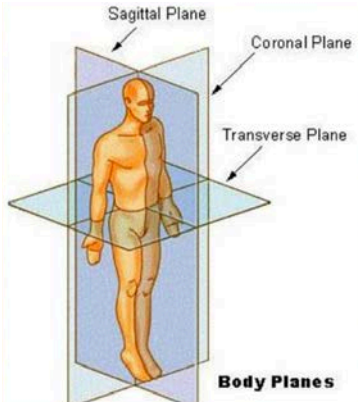

Fig. 1.10. Body planes.

Sometimes, it takes time and is subjective for the radiologists to interpret a stack of CT images from the coronal, sagittal, and axial planes in order to detect the abnormality. The anatomy-based and pathology-based knowledge are needed to interpret the 2D CT-images into medical findings. The experience of the radiologists is required to confirm the clinical result. Referring to the literature [37], surgeons/radiologists also face difficulties in identifying the horizontal fissure (RHF) in a stack of cross-sectional CT-images and take approximately 60-90 minutes to detect the RHF manually. Moreover, the challenge of CT images in breath hold technique is needed to compare the difference between two images by separating the window and the radiologists need to detect and evaluate the difference or abnormality manually. It is shown that there appears a gap between these two stages of respiratory (EI and EE). It is hard to explain the dissimilarity between these two by just comparing in two dimensions even if it is in different planes as demonstrated in Fig. 1.11.

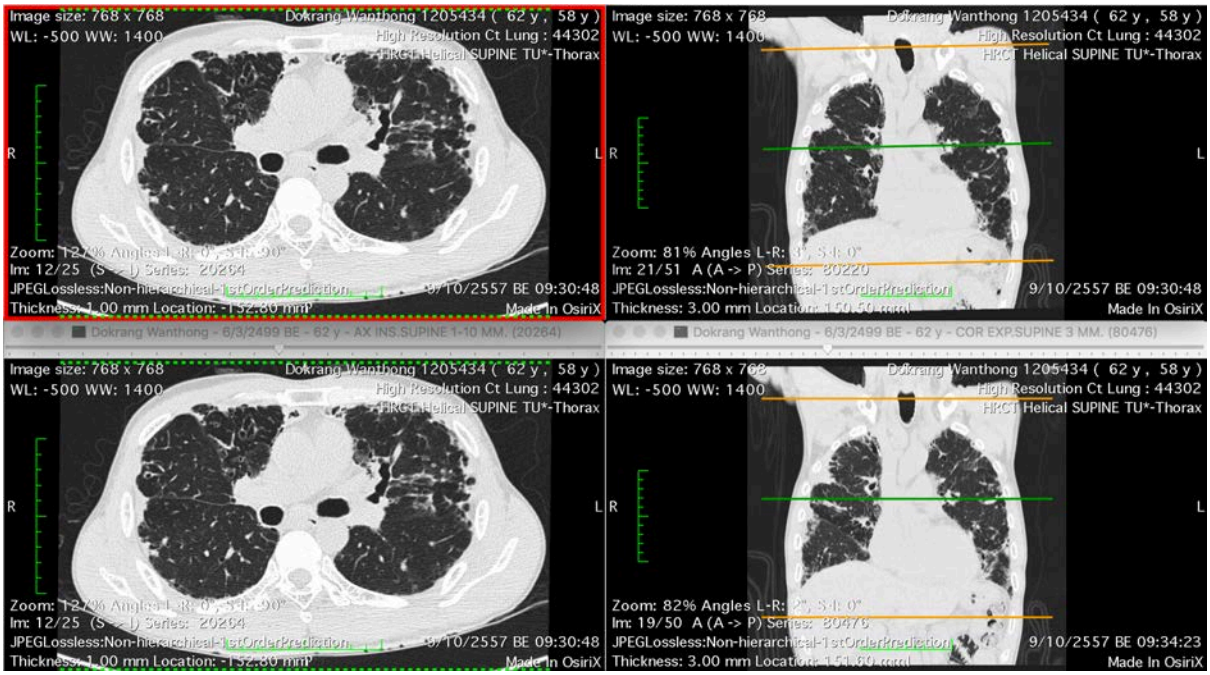

Fig. 1.11. The 2D plane of the EI and EE obstructive lung disease: (Top) EI images, (bottom) EE images.

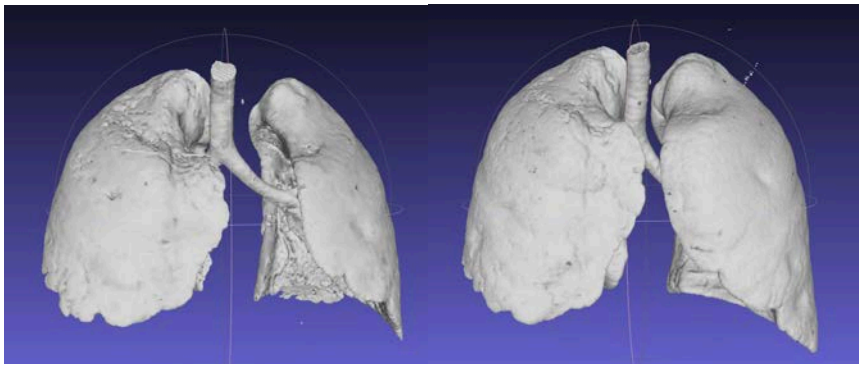

Fig.1.12. The 3D rendering images of obstructive lung disease: (left) expiratory and (right) inspiratory.

This research introduces the new dimension for data interpretation and feature representation of CT images in three dimensions with the lung-lobes separation in order to screen the lung diseases by using the inhomogeneous motion pattern as an important feature from 3D lung models as shown on Fig. 1.12.

1.3 Contribution and Significant of Study

1.3.1 Contribution to medical image processing

- New feature representation for HRCT images (EI and EE): velocity vector map of each lung lobe and its ratio (EI to EE).
- Generate predictive models based on the medical knowledge and breathing motion of the lungs.

1.3.2 Contribution to Information science

- New approach for 3D Active Contour Model in three-dimensional surface data to detect the motion and also the biophysical model for image registration.

1.3.3 Significant of this study

- Fill the gap between the medical knowledge-based and image processing and computer vision techniques by generating the predictive modelling to screening the lung diseases learning from the inhomogeneous motion of the restrictive and obstructive lung diseases.

1.4 Philosophy of this work

The analysis of the inhomogeneous motion of the 3D shape of the lung in order to diagnose the lung diseases. The velocity vector map from the End Inspiration (EI) to the End Expiration (EE) Model can be estimated by 3D Active Contour Model (3D-ACM) with automated adjusted-parameters with 3 selective feature sets. The abnormality of the movement is detected and separated into 5 lobes in order to analyze the characteristic of the lung diseases. Lastly, the hierarchy predictive modeling is applied in order to increase the efficiency of classification compared to the traditional multiclassification model.

1.5 Dissertation Organization

The introduction and background of this dissertation is described above. The motivation and problem statements are also mentioned in the First Chapter including the philosophy of this research. The other Chapters are organized as follows: related works about lung diseases analysis by using IE and EE CT-images, registration steps, 3D motion analysis, lung lobe detection, feature representation, and classification techniques are explained in the Second Chapter. The Third Chapter is about how to collect the data, to set the environment of the experiment, and to explore and generate the characteristic model to analyze lung diseases. The Fourth Chapter provides the overview of the methodology and also gets insight into each step starting from the data acquisition till the analyzation part. The next Chapter is the evaluation and the discussion of the results. The evaluation technique is also described in this Fifth Chapter. The last Chapter concludes the research story, results, and its contribution in different point of views and the future works.

Chapter 2

Related works

2.1 Overview of knowledge-based approach to lung diseases

Nowadays Machine Learning and Artificial Intelligent (AI) is popular in many research fields. In biomedical research, the feature representation of medical data is detected in order to classify the abnormality. The formal technique to analyze the diseases is pattern recognition. As described in **Chapter 1**, lung disease can be mainly separated into 2 groups: restrictive and obstructive lung disease. Analyzing the obstructive lung diseases such as Chronic Obstructive Pulmonary Disease (COPD), Emphysema, Asthma, and Small Airway Disease is found in many research articles. Referred to [6], Thoracic Quantitative computed tomographic (QCT) technique was applied to distinguish the airflow limitation problem between Asthmatic and COPD patients by using emphysema assessed based on lung density (Hounsfield Unit (HU)), air trapping detection from measuring the mean lung density expiratory to inspiratory ratio and Proximal airway percentage wall area (%WA). It was shown that HUs for normal, asthma and COPD were -937, -937, -964, the mean lung density expiratory to inspiratory ratios were 0.816, 0.852, and 0.922 and %WA were 60.3%, 62.5%, and 62.7% respectively. They found the structure-function relationship among these findings related to the identification and severity of the COPD and asthma. The challenge of this research is to identify the abnormality based on their findings to diagnose the clinical result which directly benefits the patient for the right treatment. The overlap syndrome between asthma and COPD is called (ACOS) [8]. In [8], the clinical phenotypes (symptoms, physiology, and biomarkers) are used to scale the diseases (asthma, ACOS, and COPD). The susceptibility factors (such as genetics), Environment (such as smoking, biomass exposure, pollution, infections, microbiome, and diet) were combined to

manage the airway disease including identification of specific treatment targets to optimize symptom control and reduce risks of overtreatment. As summarized in [15], ACOS is characterized by persistent airflow limitation with several features usually associated with asthma and several features usually associated with COPD. Therefore, the features shared with asthma and COPD are used to diagnose the ACOS for the proper treatment. In [11], the characteristic function to analyze ACOS was studied from CT images in the sagittal plane by showing the larger variations of the sagittal lung. The variations were lung height (measured from lung apex to the dorm of hemidiaphragm), anterior-posterior lung diameter (measured through hilum at widest point), hemidiaphragm height (measured from apex of hemidiaphragm to line connection anterior and posterior costophrenic angles), anterior sterno-diaphragm angle (measured where hemidiaphragm touches anterior thoracic wall), and retrosternal lucency (measured as maximum length of intrapulmonary septum in Axial plane). It was found that the sagittal-lung CT measurement can be used to differentiate asthma, COPD and ACOS.
However, they mentioned that this measurement still had many limitations because it cannot confirm the diagnosis result without sputum cellular profiles, airway hyper-responsiveness, and fractional exhaled nitric oxide, and etc. Other parts of the respiratory system such as the airway is used to determine lung disease such as COPD as well. In [16], they evaluated the computed fluid dynamic (CFD) inside the airway to show how the airway related to the COPD. They found that the lower branch of the airway influences the most and they also studied the recirculation of the respiratory system. They suggested that the patient with COPD or airway disease has to breathe gently in order to avoid the circulation because the re-circulation will block the air from entering the lower branch of the airway.

There is another work conducting the research on the small airway disease in COPD [10]. In [10], the HU was evaluated to detect the emphysema inside the lung by comparing the HU between EI and EE CT images. The threshold HU of EI phase is -950 and HU of EE is -856 and the EE to EI ratio of mean lung attenuation (MLA) from density histogram was determined. Moreover, the relative volume change (RVC) of different HU varying from -850 to

-950 is measured. Finally, it was found that the findings such as air trapping inside the lungs can be used to understand the pathobiology of COPD subtype.

Another feature that relates to the COPD is heart size. The lung function and heart function are associated by blood and the particles inside the blood cell such as oxygen and carbon dioxide. In [14], their experiment was set by checking hyperinflation consisting of the inspiration-to-total lung capacity ratio (IC/TLC) of the 6-min walk distance COPD patients, functional residual capacity, and residual volume. Based on their experiment result, the heart size trends to be decreased in the increasing rate of severity in COPD. The hyperinflation, therefore, is associated with the severity of the COPD.

In addition, the interpretation of HRCT images using HU is not only can determine the obstructive lung disease but also the restrictive lung diseases such as interstitial lung disease by detecting the pattern of tissue inside the lung e.g. honeycombing pattern [4], nodules (size > 3 cm) [2]. The volume of interest into nodules and nodules was analyzed in [2] in order to reduce the false positive (FP) case between masses opacity and nodules which is associated with clinical diagnosis result and their treatment.

In this research, End Inspiratory and End Expiratory CT images (EI and EE CT images) are used as a parallel input data in order to analyze and detect the inhomogeneous motion of lungs. As mentioned above, it infers that the shape and inhomogeneous motion of the lungs are associated with emphysema, air trapping, small airway disease, nodules, tissue texture inside the lungs. Therefore, the motion prediction between EI and EE CT images is used as a feature to evaluate the shape changing which refers to the different types of lung disease. The restrictive type is mostly influenced in the EI phase because the patient lost the ability to take the full inhalation. The lung size is limited based on the destroyed tissues inside. The obstructive one is significant in EE phase because the patient lacks ability to exhale caused by small airway disease or inflammation of the airway or mucus.

2.2 Literature reviews of the EI and EE lung CT images

The CT images are separated into two types: 3D CT images and 4D CT images. The fourth dimension is time. 4D-CT images are mostly used to detect the motion of the tumor while radiation in chemo treatment in order to reduce the false shooting of the radiation. The 4D-CT consists of many sets of images during natural respiratory. The guideline for taking 4D-CT may be changed based on the analysis or clinical question. On the other hand, the traditional 3D CT images use breath hold technique from End-Inspiratory to End-Expiratory (EI to EE). The use of EI and EE CT images is by analyzing the inside pattern of the tissue, airway, heart size, attenuation (HU), volume, area, diameter and etc. or using the surface and its predicted velocity vector. The literature reviews and the uses for the 3D-CT images and 4D-CT images is described in Table 2.1.

Table 2.1 The literature reviews of the data types and its segmentation scope.

References (year)	CT types	Segmentation	Lung diseases
[6]	3D-CT (EI, EE)	Coronal plane, HU	Asthma, COPD
[10] (2013)	3D-CT (EI, EE)	Volume, HU	Small airway, COPD
[11] (2017)	3D-CT (EI, EE)	Sagittal plane, HU	Asthma, ACOS, COPD
[4] (2011)	3D-CT (EI, EE)	Coronal plane, HU	Interstitial lung disease, bronchiectasis
[2] (2017)	3D-CT	Volume (VOI)	Nodules
[18] (2014)	4D-CT	Motion	Cancer
[17] (2009)	4D-CT	Motion	Cancer
[19] (2015)	4D-CT	Displacement, Deformation	Cancer
[20] (2015)	4D-CT	Biomedical model	Cancer
[22]	4D-CT	Motion	Cancer
[23] (2012)	4D-CT	Motion	Cancer
[26] (2017)	4D-CT	Motion	-

[28] (2017)	4D-CT	Motion	-
[37]	3D-CT	Oblique fissure	Lung lobes
[36]	3D-CT	Oblique fissure	Lung lobes
[35] (2009)	3D-CT	Oblique fissure	Lung lobes
[46] (2014)	3D-CT	Oblique fissure, HU volume	Lung lobes, emphysema

Based on the trend of study (from the 20th century until now) in Tab. 2.1, it can be concluded that the 3D-CT with breath hold technique is generally applied to diagnose diseases in different ways such as coronal plane analysis, sagittal plane analysis. 4D-CT images are mostly analyzed by using a 3D model to evaluate the respiratory motion (natural breathing).

2.3 Literature reviews of non-rigid registration and landmark points

Table 2.1: The literature reviews of non-rigid registration and landmark points.

References	CT types	Registration	Landmark or corresponding point
[18](2014)	4D-CT	Deformation model and a patch-based framework.	- Patch size is 32 x 32 voxels in a slice - 24 voxels overlap between patches
[17](2009)	4D-CT	Dense diffeomorphic deformations between image of all the time points	- 450 surface points
[19](2015)	4D-CT	Dynamic biomechanical model	- 21,000 linear tetrahedral elements - 75 landmarks
[20](2015)	4D-CT	Biomechanical model	- 414 landmarks - a trust-region optimizer
[22](20xx)	4D-CT	Interpolation using thin-plate-spline deformation field	- corresponding landmark calculated from the motion vectors using PCA
[23](2012)	4D-CT	Biomechanical Fast Finite Method (FEM)	- not given
[26](2017)	4D-CT	Hybrid patient-specific biomechanical model-based image registration method.	-3000 landmarks
[28](2017)	4D-CT	Bayesian registration	-300 landmarks

2.4 Literature reviews of 4D inhomogeneous motion analysis

Table 2.3 The literature reviews of 4D inhomogeneous motion analysis.

References	CT types	Motion Analysis	Comments
[18] (2014)	4D-CT	Approximate deformation and Computational fluid dynamics (CFD)	Study the change of flow pattern and pressure distribution.
[17] (2009)	4D-CT	Linear mapping function	Mapping a shape change to its corresponding image deformation.
[19] (2015)	4D-CT	Finite element method	Predict lung tumor displacement and deformation.
[20] (2015)	4D-CT	Biomedical model	Estimate patient-specific thoracic pressure value
[22]	4D-CT	Motion Vector from landmark points.	Diaphragm and rib-cage motion
[23] (2012)	4D-CT	Biomechanical Fast Finite Method	Fast predictive lung wall motion
[26] (2017)	4D-CT	Finite element method (FEM+B-spline)	Displacement compensation
[28] (2017)	4D-CT	Trajectory modelling	Motion model based on a continue time-related displacement filed by linking the displacement fields at discrete phases

2.5 Literature reviews of lung lobe segmentation

The anatomy of the left and the right lung are different. Left lung consists of 2 main lobes: left upper lobe (LUP), left lower lobe (LLL). The LUP and LLL is divided by left oblique fissure (LOF). Right lung contains 3 lobes: right upper lobe (RUL), right middle lobe (RML), and right lower lobe (RLL). The RUL and RMD is separated from the RLL by right oblique fissure and the RUL and RML are distinguished by right horizontal fissure (RHF). The characteristic and the angle of the LOF and ROF plane with respect to the Z-axis go to the similar way. The angle is approximately 45 degrees with respect to Z-axis in normal people. The RHF plane angle is approximately 90 degrees with respect to Z-axis or parallel to the XY-axis in normal people. The techniques to detect the location of the oblique fissure and horizontal fissure are commonly applied in 2D plane in sagittal and transverse plane which are described

in more details in **Chapter 1**. After the estimated location of the fissures are obtained, the next step is image verification and 3D modeling for visualizing the separated lung lobes. In [36], the adaptive fissure sweeping technique was applied to find the fissure regions and then wavelet transformation was applied to identify the fissure location and curvature within the regions. In [35], the ridgeness measure was used and 3D graph search was applied to search the optimal surface within the ROI and water shade segmentation was taken afterward to fill the ROI. However, they showed the solving problem of incomplete fissure by using a fast matching-based segmentation of a projection of the optimal surface. In addition, as explained in [046], the three fissures were detected as a 3D plane and then they found more findings such as lung density, texture, airway, blood vessel structure, ventilation, perfusion. After that they detect the low attenuation area of emphysema from each lung lobe aiming to analyze the abnormality from the different lobes. Compared to this research, the analysis of velocity vector maps is estimated and to make the model more effective and robust, the lung lobe segmentation is applied to analyze the characteristic model of each lobe. The lung diseases and medical knowledge based in anatomy and pathology is integrated to generate the analysis model to screening the lung disease for example the small airway disease will affect most in the lower lobe.

Chapter 3

Data Set and Experiment Setting

3.1 Ground Truth

The characteristics of normal lungs can be described by spirometry's metrics which are Forced Vital Capacity (FVC), Forced Expiratory Volume in 1 second (FEV1), and FEV1/FVC ratio. FVC measures the total exhaled volume after full inspiration. FEV1 measures the exhaled volume only in the first second. FEV1 can measure the elasticity of lung and the ability to exhale which can be used to analyze the obstructive and restrictive lung diseases. The relation between FVC and FEV1 can be described by using the FEV1/FVC ratio.

Group 1: Normal

The term 'Normal' means the healthy respiratory function with no past lung diseases. It has the ability to bring air into the lungs with full and deep breath without any difficulties that might reduce the amount of space in the lungs or narrow down the airway.

Group 2: Abnormal

Abnormal can be divided into 2 main sub-groups:

Sub-group Abnormal A: Obstructive Disease

As described in Chapter 1 about the pulmonary function test (PFTs), the people who have obstructive disease will have some common findings such as air trapping, small airway disease, emphysema, bronchiectasis, mucous plugging as found in Tab. 3.1. This kind of finding groups also can represent the severity of the disease and it affects the motion of the lung in each lobe while breathing such as air trapping, small airway disease, emphysema, bronchiectasis, mucous plugging

Sub-group Abnormal B: Restrictive Disease

Restrictive lung disease is commonly found in the fibrosis, atelectasis, air trapping, scar which represent the destroyed lung tissues inside. When the lung detects bacteria, virus, or fungi which are the general cause of restrictive disease, the immune system and lymphatic system and

its circulatory system will help to detect and remove or destroy the foreign substances out of the body. The part of the lung which is infected by the foreign substance can be used to predict the lung disease. The diffuse lesion that can be eliminated by the lymphatic system such as TB, silicosis. It is usually found in the diffuse lesion left at the apical part of the upper and superior of the lower lobe because in these areas the circulation of the lymphatic system does not flow as much as the other parts. In addition, the diffuse lesion that can be eliminated by the immune system such as UIP, NSIP, asbestosis, fibrosis, interstitial lung disease. Mostly it will appear at the lower lobe of the lung and also in the posterior side.

Table 3.1 The example of ground truth information for analyzing lung diseases based on its finding in each lobe.

	LEFT		RIGHT		
	LUL	LLL	RUL	RML	RLL
1	Emphysema	Emp, fibrosis	Emp, nodule	Emp	Emp, fibrosis
2	n/a	AT, fibrosis	n/a	plate atelectasis	fibrosis, AT, traction bronchiectasis
3	n/a	mucous plugging	n/a	nodule	mucous plugging
4	mild cylindrical bronchiectasis	mild cylindrical bronchiectasis	AT, mild cylindrical bronchiectasis	n/a	mild cylindrical bronchiectasis
5	n/a	n/a	n/a	n/a	n/a
6	inflammatory, ground glass opacity	AT, emp	inflammatory, ground glass opacity	n/a	AT, emp, inflammatory nodule
7	fibrosis, nodule, AT	AT	AT	AT	AT
8	n/a	n/a	n/a	n/a	n/a
9	nodule, AT	AT	calcification, nodule, AT	AT	AT
10	AT	AT	n/a	n/a	AT
11	emp, mucous plugging	Emp, mucous plugging	Emp, mucous plugging	Emp, mucous plugging, nodule	Emp, mucous plugging
12	n/a	n/a	n/a	n/a	n/a
13	AT	AT	AT	thin wall cyatic lesions scattering, AT	AT

14	traction Bronchiectasis, AT	lung fibrosis, traction Bronchiectasis, AT	AT	traction Bronchiectasis, AT	lung fibrosis, traction Bronchiectasis, AT
15	AT, interstitial fibrosis	AT, interstitial fibrosis	AT, interstitial fibrosis	AT, interstitial fibrosis	AT, interstitial fibrosis
16	AT, interstitial fibrosis	bular septal, AT, interstitial fibrosis	AT, interstitial fibrosis	AT, interstitial fibrosis	bular septal, AT, interstitial fibrosis
17	AT	AT	interstitial fibrosis, AT	AT	interstitial fibrosis, AT
18	bronchiectasis	bronchiectasis	bronchiectasis	bronchiectasis	Ground glass opacity, bronchiectasis
19	AT, mucous plugging	AT	AT, mucous plugging	AT, mucous plugging	AT
20	bronchiectasis	bronchiectasis	bronchiectasis, AT, ground glass opacity	bronchiectasis, AT	bronchiectasis, AT, ground glass opacity
21	bronchiectasis	bronchiectasis	AT, bronchiectasis	n/a	bronchiectasis
22	bronchiectasis	bronchiectasis	bronchiectasis	bronchiectasis, reticulonodular	bronchiectasis
23	ground glass opacity, mucous plugging	mucous plugging	ground glass opacity, mucous plugging	mucous plugging	mucous plugging
24	nodular, bronchiectasis	cavity lesions	n/a	n/a	n/a
25	nodular, bronchiectasis, mucous plugging	n/a	nodular, bronchiectasis, mucous plugging	nodular, bronchiectasis, mucous plugging	n/a
26	AT	AT	AT	AT	AT
27	n/a	n/a	n/a	n/a	n/a
28	bronchiectasis, AT	bronchiectasis, AT	bronchiectasis, AT	Consolidation, bronchiectasis, AT	bronchiectasis, AT
29	AT, interstitial fibrosis	AT, interstitial fibrosis	AT, interstitial fibrosis	AT, interstitial fibrosis	AT, interstitial fibrosis
30	emp, AT, bronchiectasis, nodules	emp, AT, bronchiectasis	emp, AT, bronchiectasis, nodule	emp, AT, bronchiectasis, nodule	emp, AT, bronchiectasis
31	AT, fibrosis, atelectasis	AT, lobular septal	AT	AT, atelectasis	AT, lobular septal

32	AT	AT	AT	bronchiectasis, atelectasis, AT	bronchiectasis, AT
33	n/a	mucous plugging, bronchiectasis, nodule	n/a	n/a	mucous plugging, bronchiectasis, nodule
34	AT, tree-in-bud	AT, tree-in-bud	AT, tree-in-bud	AT, tree-in-bud	AT, tree-in-bud
35	AT, fibrosis	AT	AT, fibrosis, consolidation	AT	AT
36	n/a	n/a	n/a	n/a	nodule
37	AT, fibrosis, bronchiectasis	AT	AT	AT, fibrosis, bronchiectasis	AT
38	AT, atelectasis	AT	AT	AT	AT
39	n/a	calcification, AT	ground glass opacity	n/a	AT
40	fibrosis	n/a	fibrosis	n/a	nodule
41	emp	emp	emp, nodule	emp	emp, bular septal
42	AT	AT	AT	AT	AT
43	bronchiectasis, fibrosis	bronchiectasis, mucous plugging, nodules	fibrosis	bronchiectasis	n/a
44	n/a	n/a	nodule	nodule	nodule
45	n/a	n/a	n/a	n/a	n/a
46	n/a	bronchiectasis, atelectasis	n/a	n/a	n/a
47	n/a	n/a	n/a	n/a	n/a
48	AT, atelectasis	AT	AT, mucous plugging, atelectasis	AT	AT, mucous plugging
49	AT, fibrosis, atelectasis	At, lobular septal	AT	AT, atelectasis	AT, lobular septal
50	AT	AT	AT	bronchiectasis, atelectasis, AT	bronchiectasis, AT
51	n/a	mucous plugging, bronchiectatis, nodule	n/a	n/a	mucous plugging, bronchiectatis, nodule
52	AT, tree-in-bud	AT, tree-in-bud	AT, tree-in-bud	AT, tree-in-bud	AT, tree-in-bud
53	AT, fibrosis	AT	AT, fibrosis, consolidation	AT	AT

54	inflammatory, ground glass opacity	AT, emp	inflammatory, ground glass opacity	n/a	AT, emp, inflammatory nodule
55	fibrosis, nodule, AT	AT	AT	AT	AT
56	bronchiectasis, fibrosis	bronchiectasis, mucous plugging, nodules	fibrosis	bronchiectasis	n/a
57	n/a	n/a	nodule	nodule	nodule
58	n/a	n/a	n/a	n/a	n/a
59	n/a	bronchiectasis, atelectasis	n/a	n/a	n/a
60	at, interstitial fibrosis	AT, interstitial fibrosis	AT, interstitial fibrosis	AT, interstitial fibrosis	AT, interstitial fibrosis
61	emp, AT, bronchiectasis, nodules	emp, AT, bronchiectasis	emp, AT, bronchiectasis, nodule	emp, AT, bronchiectasis, nodule	emp, AT, bronchiectasis
62	n/a	mucous plugging	n/a	nodule	mucous plugging
63	mild cylindrical bronchiectasis	mild cylindrical bronchiectasis	AT, mild cylindrical bronchiectasis	n/a	mild cylindrical bronchiectasis
64	n/a	n/a	n/a	n/a	n/a
65	n/a	mucous plugging	n/a	nodule	mucous plugging
66	AT, tree-in-bud	AT, tree-in-bud	AT, tree-in-bud	AT, tree-in-bud	AT, tree-in-bud
67	AT, fibrosis	AT	AT, fibrosis, consolidation	AT	AT
68	AT, interstitial fibrosis	AT, interstitial fibrosis	AT, interstitial fibrosis	AT, interstitial fibrosis	AT, interstitial fibrosis
69	AT, interstitial fibrosis	bular septal, AT, interstitial fibrosis	AT, interstitial fibrosis	AT, interstitial fibrosis	bular septal, AT, interstitial fibrosis
70	AT, fibrosis, bronchiectatis	AT	AT	AT, fibrosis, bronchiectatis	AT
71	AT, atlectasis	at	at	at	at
72	AT, atlectasis	at	at	at	at
73	n/a	calcification, at	ground glass opacity	n/a	at
74	fibrosis	n/a	fibrosis	n/a	nodule
75	emp	emp	emp, nodule	emp	emp, bular septal
76	n/a	n/a	nodule	nodule	nodule
77	n/a	n/a	n/a	n/a	n/a

78	n/a	bronchiectasis, atelectasis	n/a	n/a	n/a
79	AT, interstitial fibrosis	bular septal, AT, interstitial fibrosis	AT, interstitial fibrosis	AT, interstitial fibrosis	bular septal, AT, interstitial fibrosis
80	AT	AT	interstitial fibrosis, AT	AT	interstitial fibrosis, AT
81	bronchiectasis	bronchiectasis	bronchiectasis	bronchiectasis	Ground glass opacity, bronchiectasis
82	traction Bronchiectasis, AT	lung fibrosis, traction Bronchiectasis, AT	AT	traction Bronchiectasis, AT	lung fibrosis, traction Bronchiectasis, AT
83	AT, interstitial fibrosis	at, interstitial fibrosis	AT, interstitial fibrosis	AT, interstitial fibrosis	AT, interstitial fibrosis
84	AT, interstitial fibrosis	bular septal, AT, interstitial fibrosis	AT, interstitial fibrosis	AT, interstitial fibrosis	bular septal, AT, interstitial fibrosis
85	AT	AT	interstitial fibrosis, AT	AT	interstitial fibrosis, AT
86	n/a	AT, fibrosis	n/a	plate atelectasis	fibrosis, AT, traction bronchiectasis
87	n/a	mucous plugging	n/a	nodule	mucous plugging
88	emp, AT, bronchiectasis, nodules	emp, AT, bronchiectasis	emp, AT, bronchiectasis, nodule	emp, AT, bronchiectasis, nodule	emp, AT, bronchiectasis
89	AT, interstitial fibrosis	AT, interstitial fibrosis	AT, interstitial fibrosis	AT, interstitial fibrosis	AT, interstitial fibrosis
90	AT, interstitial fibrosis	bular septal, AT, interstitial fibrosis	AT, interstitial fibrosis	AT, interstitial fibrosis	bular septal, AT, interstitial fibrosis
91	mild cylindrical bronchiectasis	mild cylindrical bronchiectasis	AT, mild cylindrical bronchiectasis	n/a	mild cylindrical bronchiectasis
92	n/a	n/a	n/a	n/a	n/a
93	mild cylindrical bronchiectasis	mild cylindrical bronchiectasis	AT, mild cylindrical bronchiectasis	n/a	mild cylindrical bronchiectasis
94	inflammatory, ground glass opacity	AT, emp	inflammatory, ground glass opacity	n/a	AT, emp, inflammatory nodule
95	AT	AT	AT	AT	AT
96	AT	AT	AT	AT	AT
97	at, interstitial fibrosis	at, interstitial fibrosis	at, interstitial fibrosis	at, interstitial fibrosis	at, interstitial fibrosis
98	mild cylindrical bronchiectasis	mild cylindrical bronchiectasis	AT, mild cylindrical bronchiectasis	n/a	mild cylindrical bronchiectasis
99	n/a	AT, fibrosis	n/a	plate atelectasis	fibrosis, AT, traction bronchiectasis

100	bronchiectasis, fibrosis	bronchiectasis, mucous plugging, nodules	fibrosis	bronchiectasis	n/a

*AT=air trapping, Emp=emphysema, n/a=not specify

3.2 Programs and Experiment setting

The dataset is managed by the new index number with a label for each lung lobe in both left and right sides. The 3D rendering part is done by OsiriX MD (on macOS) with added plugins such as invert data, labels, volume calculator. The database is transferred and collected in the external hard disk to link the DICOM file to the OsiriX MD. The ROI tools, volume rendering, and surface rendering are used to generate the 3D model of the lungs. Meshlab (on macOS) is applied to reduce some noise from the 3D rendering process. Meshlab is also used to visualize the 3D model because it can easily transform, rotate, and collect the landmark points for generating the cutting plane for separating the lung lobes. After that, MATLAB 2016a is used to analyze the velocity vector by using 3D Active Contour Model. The Image Processing, Computer Vision system, 3D point cloud processing, 3-D Volumetric Image Processing, and Geometric Transformation and Image Registration toolboxes and etc. are used to analyze the lung models. Finally, the classification model is generated by Statistics and Machine Learning Toolbox.

Chapter 4

Methodology for 3D Image Analysis of Lung Diseases

This chapter explains the methodology of 3D image analysis of lung diseases using the velocity vector map evaluated by the 3D active contour model (3D ACM). The initial condition of 3D ACM is selected depending on the shape of the lung by calculating the ratio of the height from EE to EI model. Then 3D ACM is applied to generate the parametric surface and the expanding motion of the lung. The velocity vector of the lung's expanding motion is separated into 5 lobes. There are 2 lobes in the left lung and 3 lobes in the right lung. The reason we need to separate the lobe is each lobe has its movement pattern and this characteristic is extracted and analyzed for the classification model. All extracted information is used to examine and interpret lung diseases by using pattern recognition techniques. The predictive model is generated and optimized to classify lung diseases based on the motion of the lung by the integrated knowledge of pathology and medical images.

4.1 Overview of the System

The methodology is separated into 6 main parts: (1) Data Acquisition, (2) Pre-Processing, (3) Active Contour Model, (4) Velocity vector map, (5) Lung-lobe separation, and (6) Lung disease analysis. Figure 4.1 shows the overview of the system starting from the data acquisition until classification.

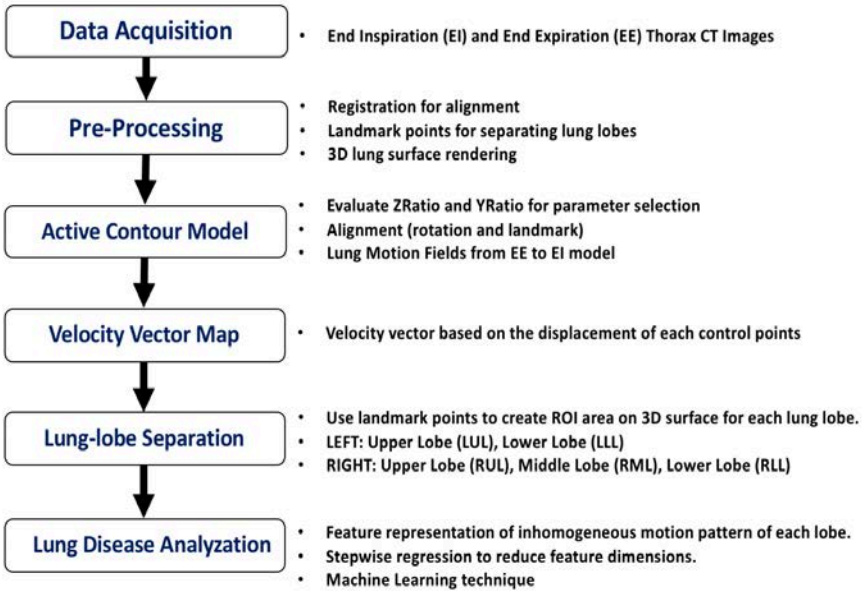

Figure 4.1 Overview of the system.

4.2 Data Acquisition

The dataset is EI and EE HRCT images in a transverse plane with 1 mm thickness. The stack of images consists of approximately 200 images or 2 mm thickness with approximately 100 images in a stack. In this research, the OsiriX MD is used to render the 3D surface model of lungs. To analyze the lung disease, the EI and EE CT images are divided into left and right models: EI_{right},EE_{right},EI_{left}, and EE_{left} as shown in Fig.4.2.

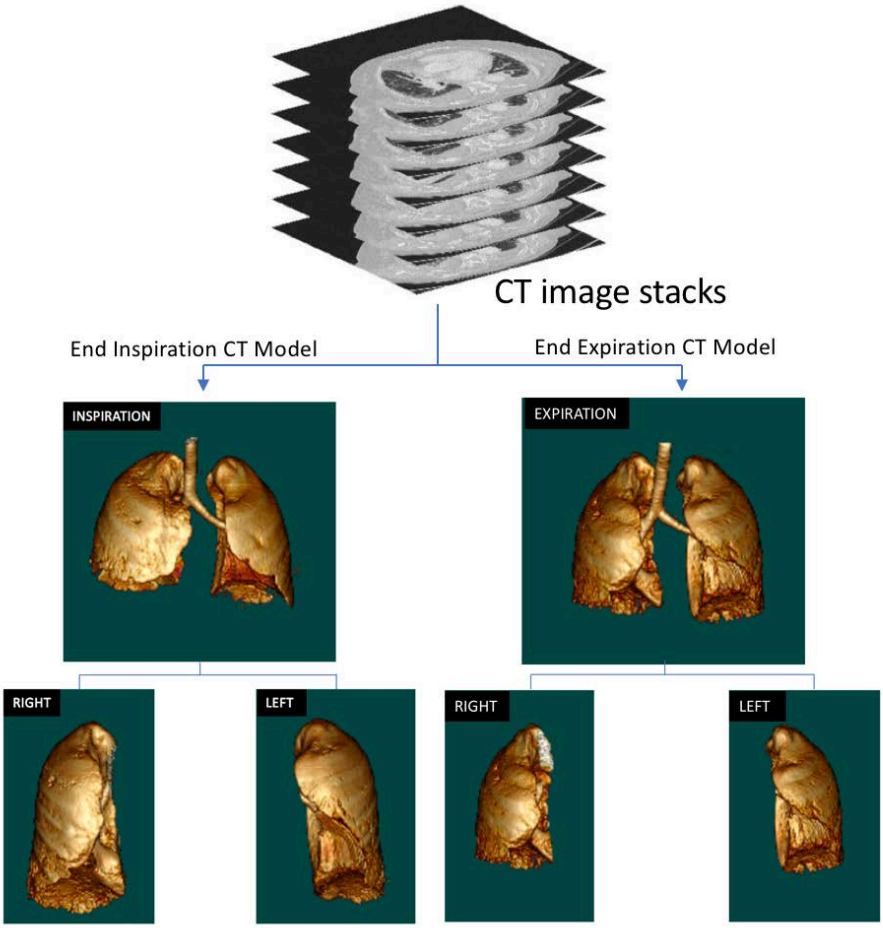

Fig. 4.2. EI_{right},EE_{right},EI_{left}, and EE_{left} models

4.2.1 DICOM File and Image Series

This research uses HRCT image series compressed in DICOM format. It contains the slice images as a stack with 512 x 512 pixels in-plane resolution. We can use HRCT images to analyze the lung diseases in both 2D and 3D planes. Fig. 4.3 shows the example of 2D segmentation of the lung region in every slice in the CT stack. The 2D plane of DICOM also has another image coordinate system represented in (*i, j, k*).

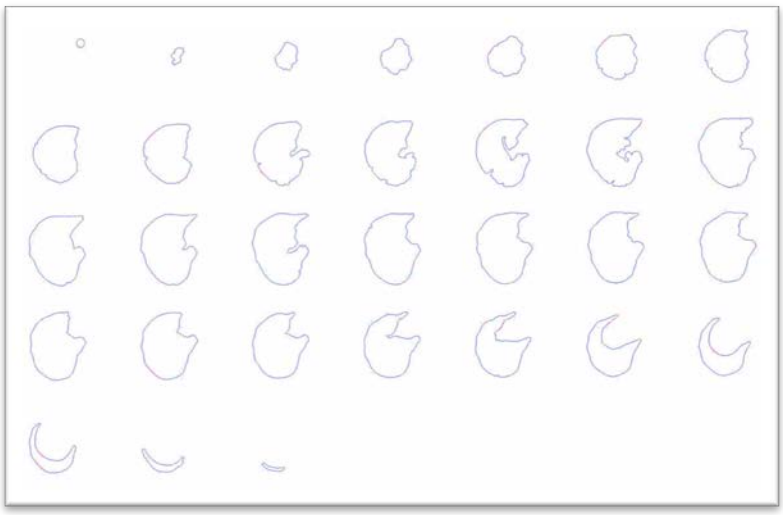

Fig. 4.3 2D ACM for region detection of lung CT images.

There are two images stacks used: (1) AX Ins. Sup. and (2) AX Exp. Sup. with 1 mm or 2 mm thickness as shown in Fig. 4.4. The 3D surface rendering is performed to generate 3D model as shown in Fig. 4.2 as EI_{right}, EE_{right}, EI_{left}, and EE_{left} models.

The image plane in anatomical and cartesian coordinates is represented in a slightly different way. For the DICOM file, the anatomical coordinate with LPS format is used. L stands for Left. P is Posterior and S is Superior. The anatomical coordinate system consists of 3 planes: axial plane (Superior-Inferior), coronal plane (Anterior-Posterior), and sagittal plane (Left-Right). Compared to the cartesian coordinate system, the axial plane is the Z-axis, the coronal plane is the Y-axis, and the sagittal plane is the X-axis.

	Anatomical Coordinate	**Cartesian Coordinate**
Superior-Inferior	axial plane	Z-axis
Anterior-Posterior	coronal plane	Y-axis
Left-Right	sagittal plane	X-axis

4.2.2 Image Planes

The transverse plane is used to visualize the cross-section of the chest. However, in the transverse plane can be separated to two positions: supine and prone. Supine transverse plane is

the stack of chest when the patient lies on his back position and prone is to lie on his stomach. Normally the data is the supine transverse plane. The prone position is token when the patient has a hard time When the data is in the prone transverse plane, the rotation of the data stack is needed before starting the analysis step.

Fig 4.4: the HRCT Image series in different plane and demonstrates the supine and prone transverse planes with 2 mm thickness.

4.2.3 Window Width and Window Level (WW and WL)

The window width and window level are the threshold number for setting the range of gray-scale. The different shades of gray level can represent the different density of body elements such as air, bone, water, fat. The suitable WW and WL for the pulmonary image are 1000 and -700 respectively. Fig. 4.4 explains the HU and specific range of the body elements density.

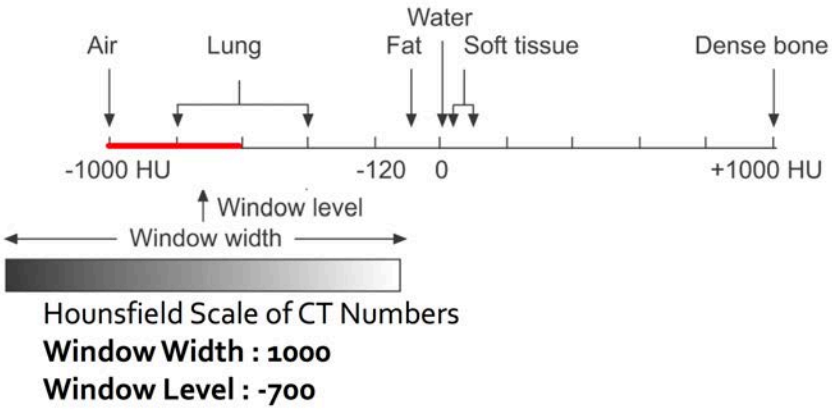

Fig. 4.4: Hounsfield scale and WW/WL setting.

4.3 Preprocessing

For the preprocessing step, the image preparation such as noise reduction and smoothen surface is performed. To reduce the segmentation error and reduce noises in further feature detection steps, the preprocessing is a must to concern.

4.3.1 Noise Deduction from Small Bronchi

The noise from the bronchi inside the lung needs to be removed before rendering the 3D surface model. First, the WW and WL are set to clearly show the pulmonary elements. Then the invert filter is performed to convert the intensity from -1024 to 1024 and from 1024 to -1024. (black and white colors are represented in -1024 and 1024 respectively) Then the ROI is applied to the pulmonary area and converts the intensity inside the ROI into 1024 as demonstrated in Fig. 4.5 (right).

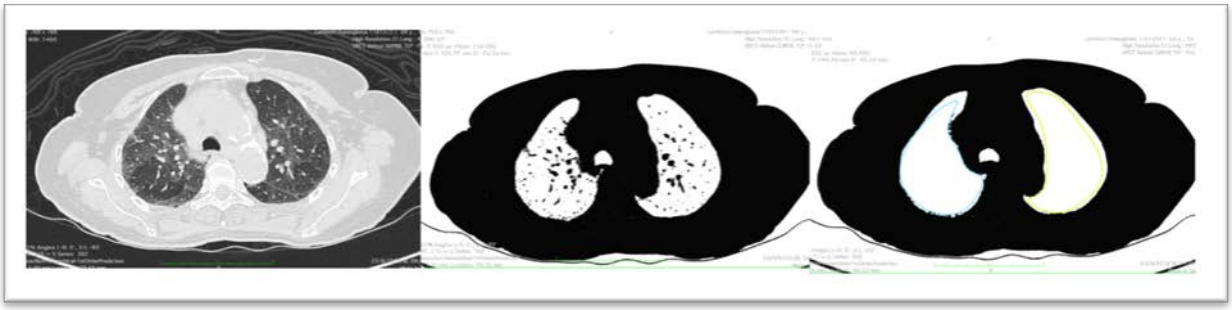

Fig. 4.5 Noise deduction process: (left) WW and WL setting, (middle) invert filter, and (right) removing noise inside the lung.

4.3.2 3D Surface Rendering

After removing noises, the volume rendering is used to generate a 3D model from the stack of CT images. Some unwanted areas are also removed such as the main airway. Then, the left and the right lungs are separated. After that, the 3D volume rendering is applied to each lung. Finally, 4 lung models are generated: EI_{right},EE_{right},EI_{left}, and EE_{left} as shown in Fig 4.6 and the main airway is already removed.

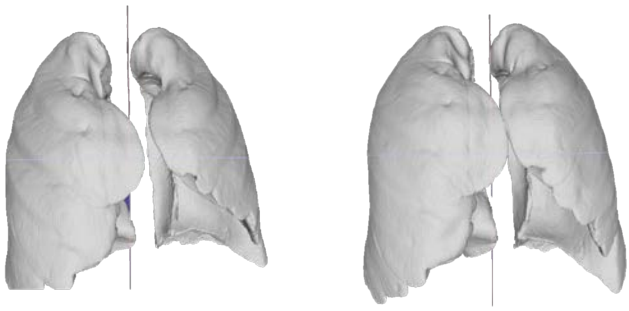

Fig. 4.6. Lung model: (left) End-Expiratory (EE), (right) End-Inspiratory (EI).

4.3.3 Resampling Surface

To reduce the time consuming, the elements of the surface are reduced to 6,000 - 10,000 elements depending on the size of the lung. As mentioned in Chapter 2, some literature shows that 3,000-10,000 elements are acceptable to estimate the motion of the lung without losing important information such as the sharp edge at the lower lobe.

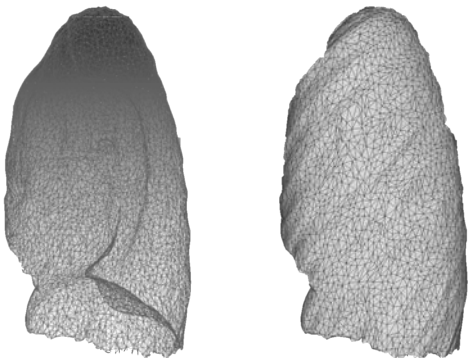

Fig. 4.7 Resampling 3D surface model to 10,000 vertices.

4.3.4 Thoracic landmark points

The landmark points are used to separate the lung lobes by using 3 sets of cutting plane: **ROF** (R_{OF1}, $R_{OF2,}$ R_{OF3}), **RHF** ($R_{HF1,}$ $R_{HF2,}$ R_{HF3}), and **LOF** (L_{OF1}, $L_{OF2,}$ L_{OF3}). The cutting plane is used to represent the oblique fissure on the lung. The right lung has 2 oblique fissures to separate 3 lobes which are Right Oblique Fissure (ROF) and Right Horizontal Fissure (RHF). The left lung

has only one oblique fissure called Left Oblique Fissure (LOF). The thoracic landmarks of ROF, RHF and LOF are represented in Fig. 4.8 and Table 4.1.

Table 4.1 The location of landmark points

Fissures	Landmark points	Anatomical location
ROF	R_{OF1}	Spinal cord: T3
	R_{OF2}	6^{Th} rib at midclavicular line
	R_{OF3}	6^{Th} rib at midclavicular line
RHF	R_{HF1}	4^{Th} rib
	R_{HF2}	5^{Th} rib
	R_{HF3}	5^{Th} rib
LOF	L_{OF1}	Spinal cord: T3
	L_{OF2}	6^{Th} rib at midclavicular line
	L_{OF3}	6^{Th} rib at midclavicular line

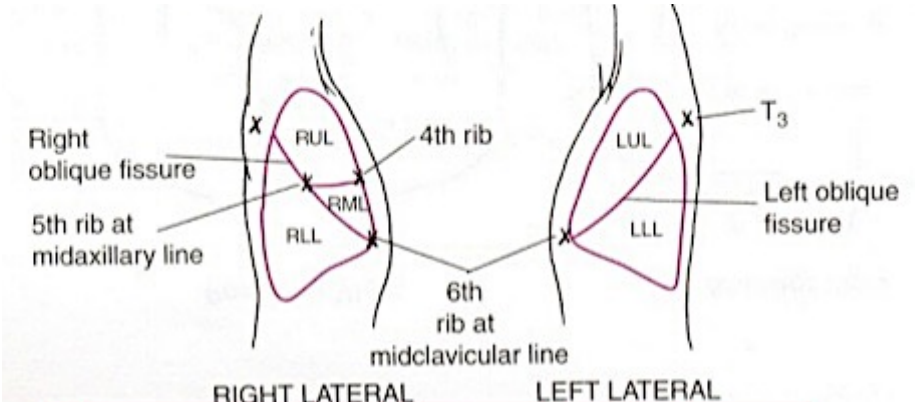

Source: https://www.slideshare.net/AliMohamedAziz/thoracic-lung-assessment

Fig. 4.8. The thoracic landmarks of ROF, RHF and LOF

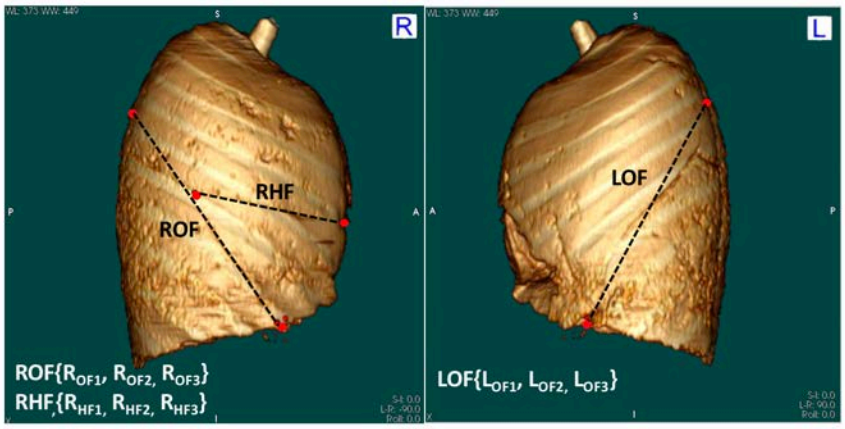

Fig 4.9 Representation of landmark points and 3 oblique fissures (RHF, ROF, and LOF) on 3D model: (left) right lung and (right) left lung.

Fig. 4.9 shows the example of landmark points on the real 3D model. The cutting plane is generated by the points and then uses the cutting plane to separate the surface of interest. This step will be applied after detecting the expanding motion of the lung by 3D ACM.

4.4 3D Active Contour Model (3D ACM)

The 3D ACM is used to detect the velocity vector map of the expanding motion of the lung. First, the parameter setting has to be simulated to find the best fit parameter for the 3D lung model. However, there is a challenging point on various sizes of lungs.

The setting of 3D ACM, the alignment is applied to set the environment for the 3D motion prediction technique. After that, the 3D parametric surface model has to be robust to the different types of data. Therefore, the parameters of 3D ACM for adjusting internal and external forces are adaptable depending on the Z_{ratio} which sketchily explains the shape of the lungs.

4.4.1 Alignment

For the alignment, the apex part of the lung is detected. The anatomy in Fig. 4.11 represents the location of the apex part which is in the upper most of lungs. Fig. 4.10 shows the misaligned models between EE and EI. The top most point of the EI phase is detected in order to be the reference point for alignment of the EE model.

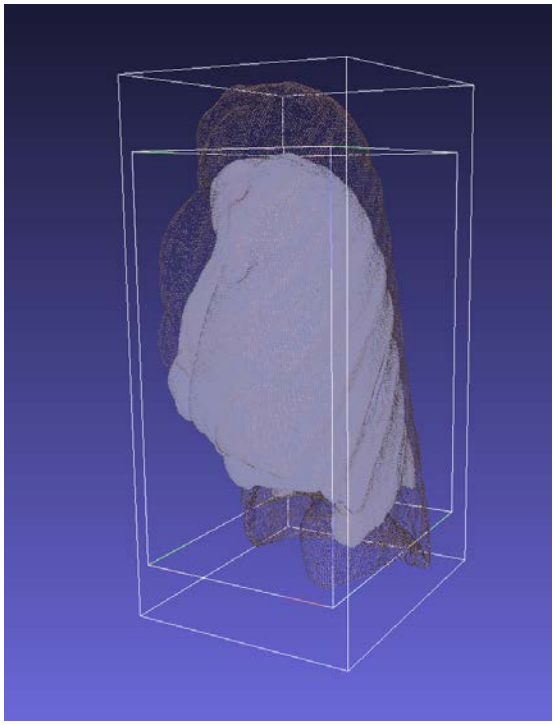

Fig. 4.10. The misaligned of 3D lung models from EI and EE phases.

4.4.2 3D Parametric Active Contour Model

The 3D ACMs are generally used as a non-rigid segmentation-based technique, especially in biomedical images. The concept of 3D ACM is to minimize the internal and external energies, and the final evaluation of the active contour will be stopped by the desired boundary of the target. In this study, the velocity vector map of the respiratory motion starting from the EE to EI phase is detected by estimating the control point on 3D ACM technique. The apex part of the lung is detected and assigned as the reference point for aligning the model. After that, the parameters of the 3D ACM for adjusting internal and external forces are set due to the sensitivity to the shape such as a sharp edge. Therefore, they are adaptable depending on the $\boldsymbol{Z_{ratio}}$ which represents the shape of the lungs.

The 3D Parametric Active Contour Model is performed to estimate the velocity vector between the EE and EI lung models. A mesh represents the control points of the 3D active contour. The energy function in 3D ACM develops the parameter function to control the control points in more dimensions as $\boldsymbol{v}: [\mathbf{0},\mathbf{1}] \times [\mathbf{0},\mathbf{1}] \rightarrow \mathbb{R}^{\mathbf{3}}$. The 3D contour is described by a function of *v*. The contour is placed on an image as $\boldsymbol{f}: \mathbb{R}^{\mathbf{3}} \rightarrow \mathbb{R}$. The snake model combines

the internal energy $\boldsymbol{E_{int}}$ and external energy $\boldsymbol{E_{ext}}$into $\boldsymbol{E = E_{int}(v) + E_{ext}(v)}$. The 3D image force concerns the movement in 3 directions of the parametric curve in $\boldsymbol{E_{int}(v)}$. Therefore, the parameter function $(\boldsymbol{v = v(s,r) = [X(s,r), Y[s,r], Z(s,r)]})$ is added to control the corresponding points (or the control points) where $\boldsymbol{X, Y, Z}$ are the corresponding coordinate function of the surface.

The internal energy $\boldsymbol{E_{int}(v)}$ can be expressed as

$$\boldsymbol{E_{int} = \iint [\alpha_s |v'_s|^2 + \alpha_r |v'_r|^2] + [\beta_s |v''_{ss}|^2 + \beta_r |v''_{rr}|^2 + \beta_{sr} |v''_{sr}|^2] \, dsdr}$$

where $\boldsymbol{\alpha_s}$ and $\boldsymbol{\alpha_r}$ denote the elasticity, respectively, $\boldsymbol{\beta_s}$ and $\boldsymbol{\beta_r}$ are the corresponding rigidities, and $\boldsymbol{\beta_{sr}}$ is the resistance to twist.

The external energy $\boldsymbol{E_{ext}(v)}$ is the image force of the boundary. In this work, the EI model is modified from the 3D surface (EI model) to 3D matrix of contour point by setting the boundary of $\boldsymbol{I_{EI}(x, y, z) = 1}$ and the inner and outer of a closed parametric surface (EE model) are set as 0. The $\boldsymbol{E_{ext}(v)}$ represents by $\boldsymbol{E_{image}(v)}$. $\boldsymbol{E_{image}(v)}$ shows the features of the EI model such as the boundary and represented it by potential force fields or the gradient of the image $\boldsymbol{\nabla p(v, f)}$ under the closed plane conditions. Next, the energy $(\boldsymbol{E = E_{int}(v) + E_{ext}(v)})$ is minimized by using the Euler-Lagrange equation to find the *v* that satisfies the equation balances the internal force and image force. When all energies are balanced, the total energy is minimum as shown.

$$\boldsymbol{[\alpha_s |v'_s|^2 + \alpha_r |v'_r|^2] - [\beta_s |v''_{ss}|^2 + \beta_r |v''_{rr}|^2 + \beta_{sr} |v''_{sr}|^2] = -\nabla p(v, f)}$$

The internal energy $\boldsymbol{E_{int}(v)}$ and its minimizing equation are set by using the 3D mesh of EE model. The characteristic of the internal force is to control the expanding motion of the parametric curve. The weighted parameters such as $\boldsymbol{\alpha}$ and $\boldsymbol{\beta}$ are used to control the tension and rigidity of the parametric curve. Fig. 4.12 shows examples of when the energy is over controlled and cannot stop at the boundary.

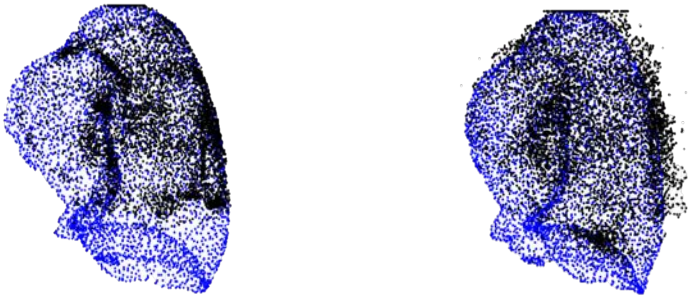

Fig. 4.12 The example when the magnitude of velocity and acceleration is unbalanced.

To generate 3D images from point clouds, the idea is by generating the squared zeros matrix in 3D in the same size as the EI model in *x, y, z* direction and sketching the point cloud into the zeros matrix. The 3D image of the EI model is now represented in 3D box containing 0 value for background and 1 for the object which is the EI model as shown in Fig.4.13.

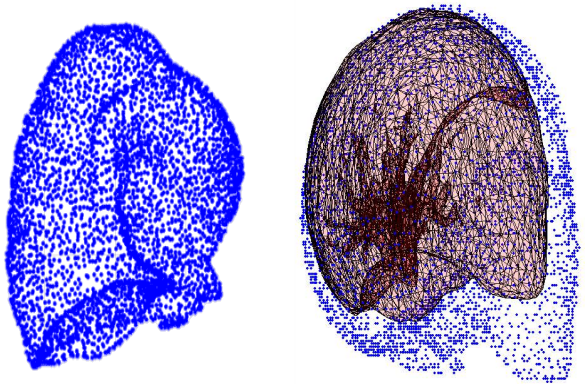

Fig 4.13 (left) transform 3D point cloud to 3D image, (right) the initial position of EE and EI models

To solve this problem as shown in Fig. 4.12, the weighted parameters of the contour and image are estimated based on the conditions for each model calculated by Z_{ratio} equation. The internal energy $\boldsymbol{E_{int}(v)}$ discourages stretching and bending of the contour while the image potential force pulls, pushing the contour toward the desired image boundary. The effect of shape and size of the lung is used the adaptive parameter technique to find the suitable parameter. Due to the complexity of the parametric contour and the potential force fields, the parameters are allowed to adapt, depending on the individual shape of a lung as shown in Fig.

5. Therefore, the additional step before applying 3D ACM is to measure the diameter of the lung in $\boldsymbol{x, y, z}$ directions. The $\boldsymbol{Z_{ratio}}$ is introduced to distinguish the different sets of shape (represented by range) estimated by the ratio of diameter EI to EE on the Z-axis as shown in Z_{ratio} equation. The shape and size of the lung is separated into 3 sets based on the data set of this study and then the weighted parameters are assigned each set called $\boldsymbol{PARAM_1}$, $\boldsymbol{PARAM_2}$,and $\boldsymbol{PARAM_3}$. When the $\boldsymbol{Z_{ratio}}$ is higher than 1.2, $\boldsymbol{PARAM_1}$ is applied, the challenge of $\boldsymbol{PARAM_1}$ is the sharp edge in the lower lung, the balloon force and GVF are tuned. $\boldsymbol{PARAM_2}$ represents the normal or slightly abnormal lungs where $\boldsymbol{Z_{ratio}}$ is between 1 to 1.2. $\boldsymbol{PARAM_3}$ is the abnormality case where it mostly appears in patients with air trapping problems (obstructive lung disease). Fig. 4.15 also demonstrates the 3D models at 3 different ranges of diameter. The $\boldsymbol{PARAM_s}$ consists of the weight of the image edge energy, image force, Gradient Vector Flow, and snake energies. They control the expanding and stop conditions of the deformable model from reaching the outer boundary.

Before starting the minimization step, the parameter setting of the contour and image is estimated based on its condition for each model calculated by Eq. (6-7). The internal energy discourages stretching and bending of the contour while the image potential force pulls, pushing the contour toward the desired image boundary. Due to the complexity of the parametric contour and the potential force fields based on the shape of the lung, the parameter setting is adaptable depending on the how much difference between the IE and EE especially at the lower lobes as shown in Fig. 4.14. Therefore, before applying the ACM, the length of the lung is determined. Z_{ratio} is the length ratio of EI to EE in Z-axis. When Z_{ratio} is higher than 1.2, the $PARAM_1$ is used. Fig. 4.15 demonstrates the 3D models with different ranges of Z_{ratio}. The structure of the $PARAM_1$ consists of the weight of image edge energy, image force, Gradient Vector Flow, and snake energies. It is to control the expanding and stop condition of the deformable model to reach the outer surface.

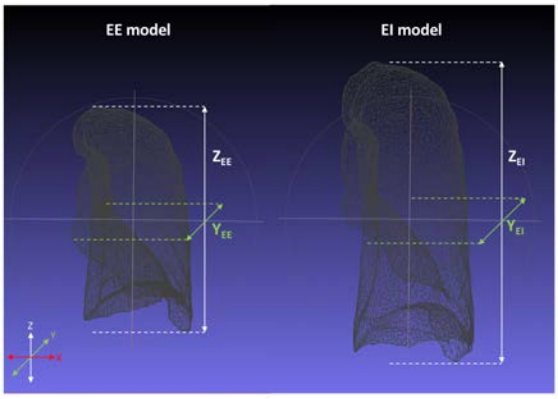

Fig. 4.14 Z_{ratio} estimation from EI and EE models.

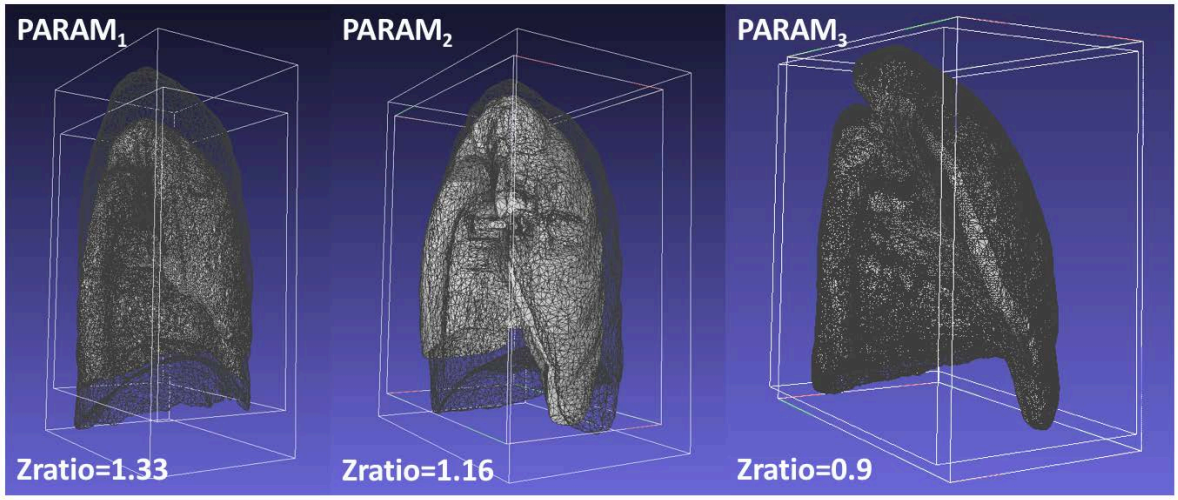

Fig4.15: Example of data set belonging to $PARAM_1$, $PARAM_2$, and $PARAM_3$

Z_{ratio} is estimated as following equation:

$$ZRatio = \frac{|Max_{ins}(EI.z) - Min_{ins}(EE.z)|}{|Max_{exp}(EI.z) - Min_{exp}\ (EE.z)|}$$

Where $|\mathbf{max}(\boldsymbol{EI.z}) - \mathbf{min}\ (\boldsymbol{EI.z})|$ represents the diameter in Z direction of EI model and $|\mathbf{max}(\boldsymbol{EE.z}) - \mathbf{min}\ (\boldsymbol{EE.z})|$ is the diameter in Z direction of EE model. The weighted parameter function depends on the range of $\boldsymbol{Z_{ratio}}$as explained below:

Parameter setting function will depend on the range of Z_{ratio} as explained below:

$$Zratio(x) = \begin{cases} PARAM_1, & x \geq 1.2 \\ PARAM_2, & 1 < x < 1.2 \\ PARAM_3, & x \leq 1 \end{cases}$$

Table 4.2. The parameter setting structure of $PARAM_1$, $PARAM_2$, and $PARAM_3$

	$PARAM_1$	$PARAM_2$	$PARAM_3$
Iterations	60	60	40
Alpha(α)	0.5	0.5	0.5
Beta (β)	0.7	0.7	0.7
W_{line}	0.5	0.5	0.5
W_{edge}	12	12	5
Kappa (κ)	10	10	10
Lambda (λ)	0.9	0.9	0.9
W_{GVF}	0.2	0.2	0.2
Delta (ll,)	10	5	0.1

To overcome some problems as shown in Fig. 4.12, Balloon Force and Gradient Vector Flow (GVF) are considered to adjust the parametric surface. These two forces help force the surface to reach the target boundary and also control the inflation force to stopped by the outer boundaries.

4.5 Velocity vector map

The velocity vector is evaluated from the corresponding points on EE model represent by 3D mesh called FV and FV.vertices is demonstrated the contour points of the active contour curve. The structure of FV contains FV.faces with a facelist (Nx3) and FV.vertices with (Nx3) vertices list. The velocity vector map is generated by the accumulating of the velocity and acceleration pixel by pixel by the active contour as shown in the $d(FV.vertices' - FV.vertices)$

$$d(x', y', z' : x, y, z) = \sqrt{(x' - x)^2 + (y' - y)^2 + (z' - z)^2}$$

The magnitude and direction from $\boldsymbol{FV.vertices}$ to $\boldsymbol{FV.vertices'}$ is a velocity vector where $\boldsymbol{FV.vertices'}$ is the stopping point (EI phase) and *FV.vertices'* is the starting point (EE phase). In this research, $\boldsymbol{d(\Delta FV.vertices)}$ is used to analyze the inhomogeneous motion pattern of

the lung. The velocity vector map calculated by $\boldsymbol{d}(\Delta \boldsymbol{FV}.\boldsymbol{vertices})$ is managed as a feature of the classification model.

4.6 Lung Lobe separation

Until this step, the velocity vector map calculated by $\boldsymbol{d}(\Delta \boldsymbol{FV}.\boldsymbol{vertices})$ is managed as a feature to the classification model. The lung lobe separation is applied to simplify the features.

4.6.1 Landmark Points and plane generation

Point based registration of oblique fissures and horizontal fissure in order to differentiate lung lobes based on its anatomical characteristic. The idea is to use the plane to separate the lung lobe. It is shown in the literature that the fissures appear naturally as 3D surfaces separating adjacent lung lobes. In some works, they combined the segmentation in 2D and 3D as a hybrid approach in order to fill in an incomplete and disrupted fissure automatically [37]. However, in this research, it is just the approximate surface of each lobe based on its anatomical characteristic. The human lungs are divided into 5 distinct anatomic compartments called lobes which are separated by the pulmonary fissures. The left lung consists of the upper and lower lobes, which are separated by the oblique or major fissure.

$\text{Lung}_{\text{Left}}$ = {Left Upper Lobe (LUL), Left Lower Lobe (LLL)}

$\text{Oblique fissure}_{\text{Left}}$ = {Left Oblique Fissure (LOF)}

The right lung consists of the upper, middle and lower lobes: the upper and middle lobes are separated by the horizontal or minor fissure; both upper and middle lobes are separated from the lower lobe by the right oblique (major) fissure.

$\text{Lung}_{\text{Right}}$ = {Right Upper Lobe (RUL), Right Middle Lobe (RML), Right Lower Lobe (RLL)}

$\text{Oblique fissure}_{\text{Right}}$ = {Right Horizontal Fissure (RHF), Right Oblique Fissure (ROF)}

The technique to separate each lobe is using the cutting plane and generating the cuboid to select the region of interest (ROI). To localize the cutting plane, there are three landmark points as explained in section above. The cutting plane is generated and then the cuboid is

created to select the region of interest (ROI). To localize the cutting plane, there are three landmark points as explained above. To create the plane, the normal vector $\vec{\boldsymbol{n}} = [\boldsymbol{a}, \boldsymbol{b}, \boldsymbol{c}]$ needs to be determined by crossing two vectors on the plane ($\boldsymbol{ax} + \boldsymbol{by} + \boldsymbol{cz} + \boldsymbol{d} = \boldsymbol{0}$). After we obtain the cutting plane, the angle of rotation could be calculated. The idea of angle of rotation is from the literature [035]. It is found that on sagittal views, the oblique and horizontal fissures are oriented at approximately 45 degrees and 90 degrees with respect to the Z-axis as shown in Fig. 4.16.

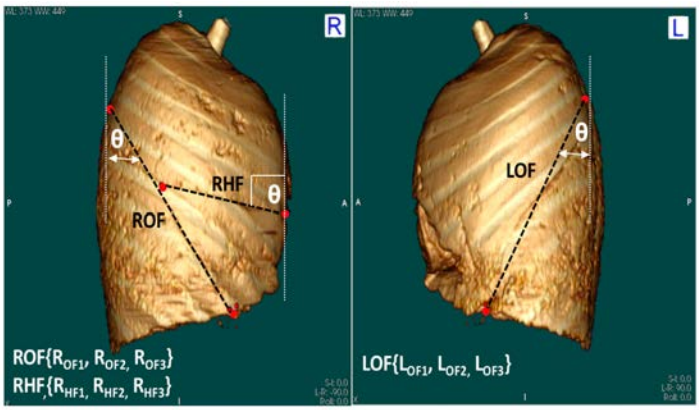

Fig. 4.16. The oblique and horizontal fissures are oriented at approximately 45 degrees and 90 degrees with respect to the Z-axis.

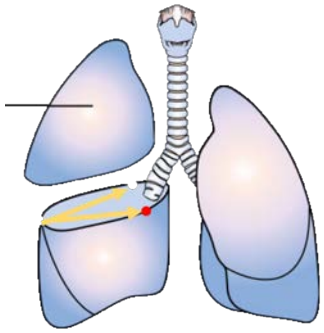

Fig. 4.17 the landmark points and its cutting plane.

The point cloud data is rotated based on that degree of rotation to select the ROI as shown in Fig. 4.19.

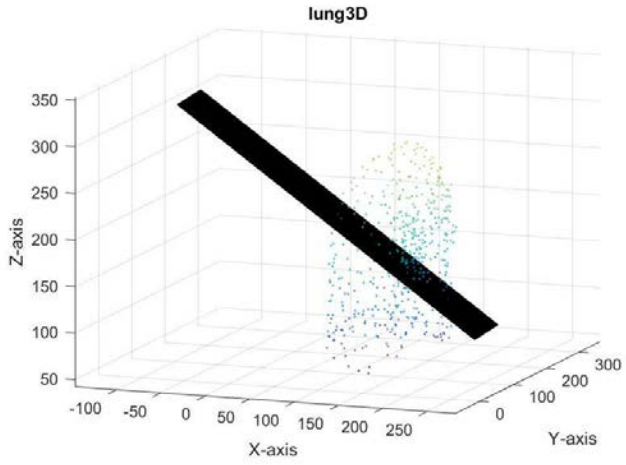

Fig. 4.18 The cutting plane of LOF in the left lung.

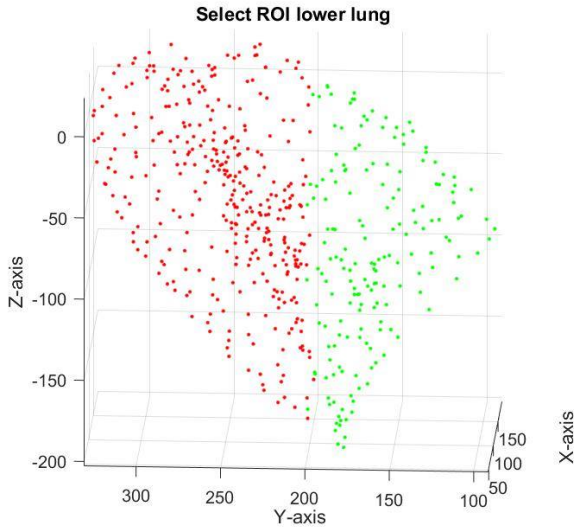

Fig. 4.19 Rotation of point cloud for cuboid ROI selection.

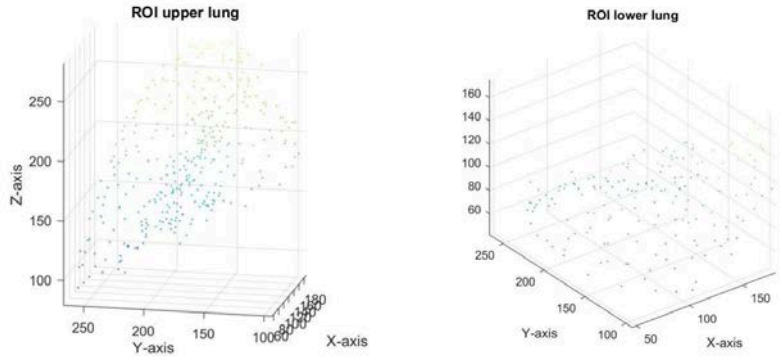

Fig. 4.20 The ROI of LUL and LLL.

4.6.2 Lung lobe separation for the right lung

For right lung separation, it is more complicated than the left lung because it consists of two fissures: RHF and ROF. Firstly, the ROF is performed by cutting RLL out of RUL and RML. Second, the RHF is generated and divides the RUL from RML. The step to generate the cutting plane and cuboid ROI is written in the Section 4.6.1 and shown in Fig. 4.16-21.

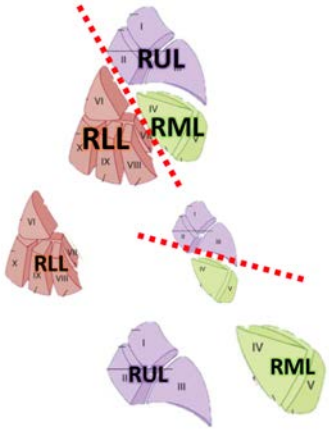

Fig. 4.21 Lung lobe separation for the right lung.

4.6.3 Lung Lobe separation for the left lung

The step to generate the cutting plane and cuboid ROI of the left lung is written in the Section 4.6.1 and shown in Fig. 4.16-20 and 4.22.

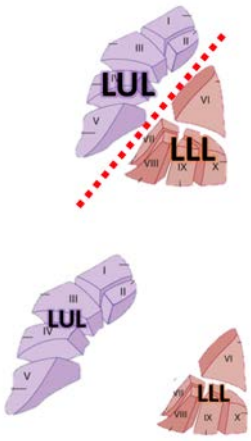

Fig. 4.22 Lung lobe separation for the left lung.

4.7 Feature representation

4.7.1 Bag-of-words (BOW) model

The BOW model is a simplifying representation of complicated features to the same dimension for feeding to the machine learning technique as training and testing data. The velocity vector with different number of control points is applied to the BOW model to simplify the dimension of information into accumulated histogram as compared in Fig. 4.23.

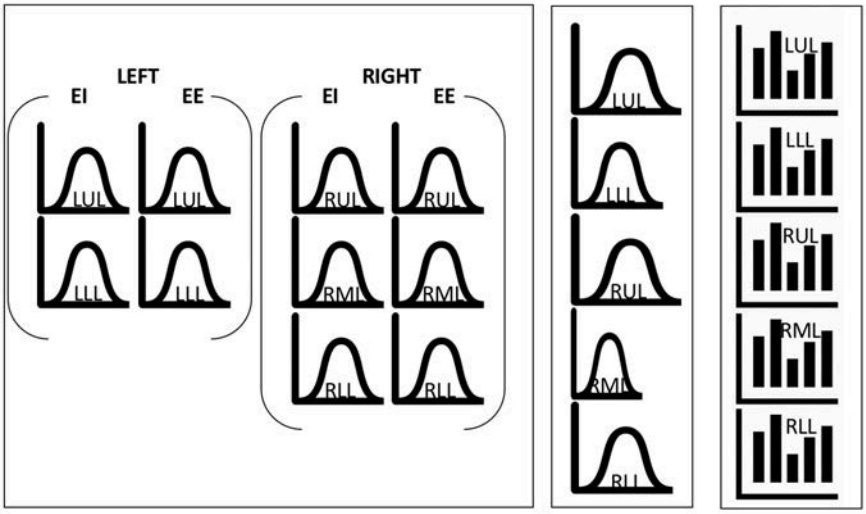

Fig. 4.23 Feature presentation from the velocity vector map to the bag-of-words.

4.8 Feature analysis and classification

4.8.1 Neural Network

The velocity vector map calculated by $\boldsymbol{d}(\Delta \boldsymbol{FV}.\boldsymbol{vertices})$ is used to analyze the expanding motion of lung. After applying lung lobe separation, there are 5 sets of lung lobes: $\boldsymbol{Lung_{Left}} = \{\boldsymbol{LUL}, \boldsymbol{LLL}\}$ and $\boldsymbol{Lung_{Right}} = \{\boldsymbol{RUL}, \boldsymbol{RML}, \boldsymbol{RLL}\}$. The complex features are simplified by using bag-of-words (BOW) model to represent in the same dimension. The velocity vector with a different number of control points is applied to the BOW model to simplify the dimensional information into an accumulated histogram represented by $\boldsymbol{d}(\Delta \boldsymbol{FV}.\boldsymbol{vertices})$. The vector set of lung lobes are obtained called visual velocity vectors. After that the normalization ($\boldsymbol{x'_i} = \left(\frac{\boldsymbol{x_i} - \boldsymbol{x_{min}}}{\boldsymbol{x_{max}} - \boldsymbol{x_{min}}}\right)(\boldsymbol{x'_{max}} - \boldsymbol{x'_{min}}) + \boldsymbol{x'_{min}}$) is applied to each visual velocity vector in order to deal with distribution of data where $\boldsymbol{x'_i}$ is the actual input feature, $\boldsymbol{x_{min}}$ and $\boldsymbol{x_{max}}$ are the minimum and maximum value of input feature and $\boldsymbol{x'_{min}}$ and

x'_{max} are the minimum and maximum target range of input feature which is [0,1]. Next, the machine learning techniques are: Artificial Neural Network (ANN)

In the ANN model, the number of hidden layers (N_L) is set as 20 based on the N_i and N_o. For the number of hidden neurons (N_N), there are many rules of thumb for calculating N_L such as method [18] $N_n = \sqrt{N_i N_o}$ where the input neuron and output neuron represent by N_i and N_o, method [17], $N_n = 2^{N_i} - 1$, method [16], $N_h = \frac{2^{N_i}}{N_i} + 1$. In this research, we optimize the performance and $N_n = \sqrt{N_i N_o} + 1$ are used for setting the hidden neurons. The activation function of the output layer is TanH function ($TanH = \frac{2}{1+e^{-2x}} - 1$) which has range values between (0,1).

4.8.2 Classification

The predictive model is mainly separated into three sub-modules. **The first module** is to separate the normal and abnormal patient by using Z_{ratio} and Y_{ratio} combined to the motion feature of each lung as shown in Fig 4.23. Secondly, the lung diseases are divided into obstructive and restrictive lung diseases by using **Module 2.** To separate the obstructive and restrictive lung diseases, the inspiratory and expiratory phase of normal people is used to analyze the similarity in order to distinguish them as shown in Fig. 4.26. Finally, **Module 3** in Fig. 4.27, the training feature is rearranged in order to detect the inhomogeneous motion pattern based on the causes of diseases which are also related to the motion in each particular lobe.

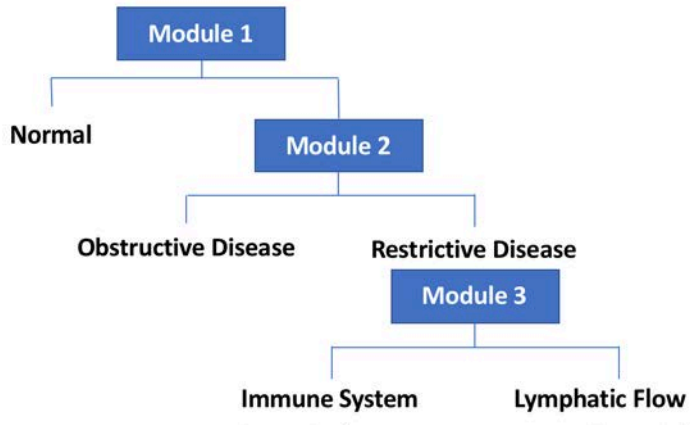

Fig. 4.24 The predictive model.

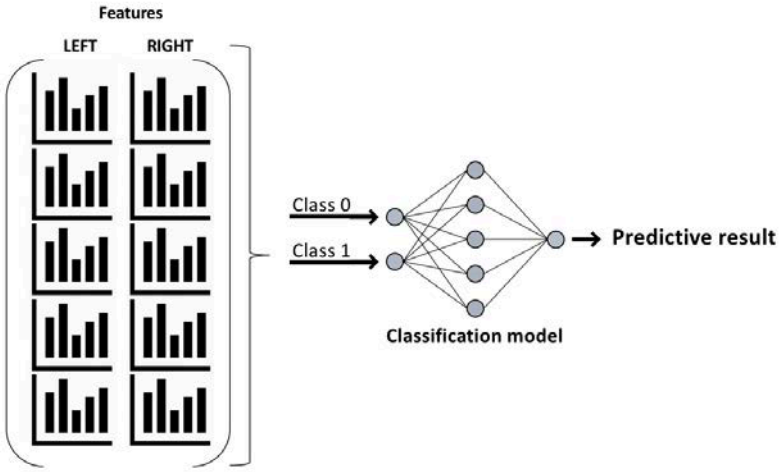

Fig 4.25. Module 1: To classify normal and abnormal lungs.

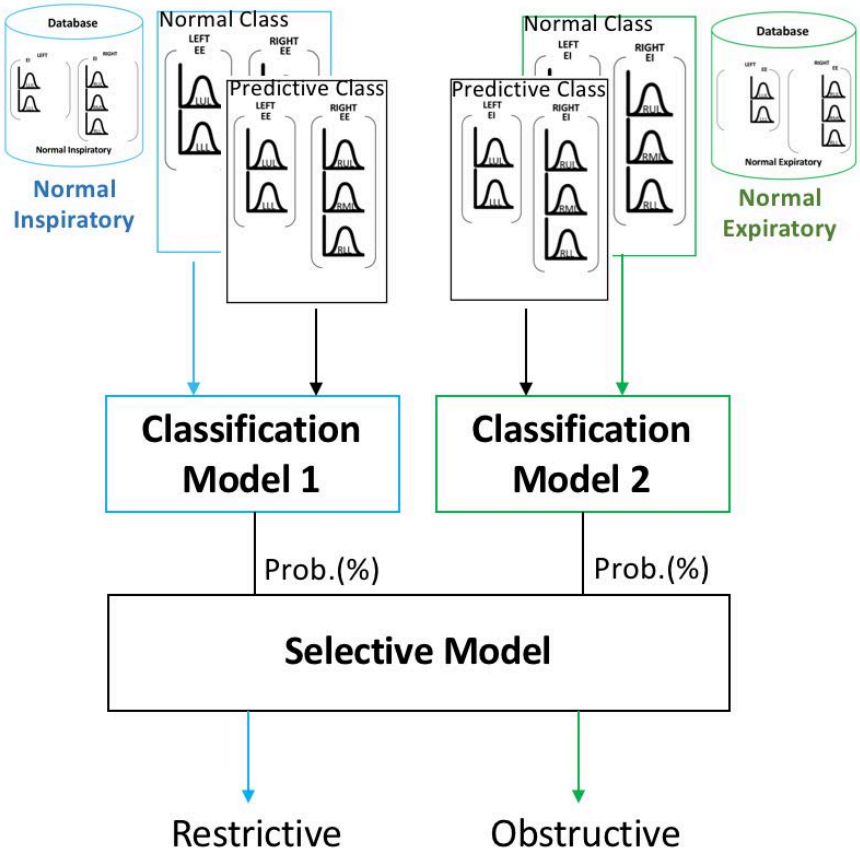

Fig 4.26. Module 2: To classify obstructive and restrictive lungs.

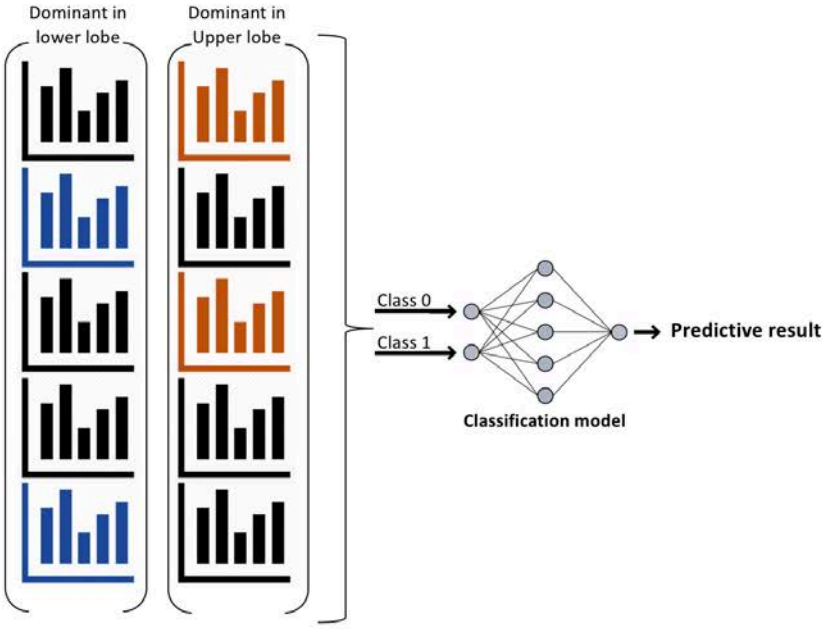

Fig 4.27. Module 3: To classify lung diseases that are caused by immune system or lymphatic system.

Chapter 5

Evaluation and Discussion

5.1 Evaluation Techniques

The confusion metric in Table 4 is used to evaluate the performance of the predictive model by accumulating the result from Module 1 to Module 3. The **Weighted Average Sensitivity and Specificity ($SENS_{Avg}$** and **$SPEC_{Avg}$) are introduced to overcome the imbalanced data problem.**

Table 5.1 Confusion Matrix of the predictive model.

Predictive Model		**Actual Classification**	
		0	**1**
Predictive Result	**0**	True Negative	False Negative
	1	False Positive	True Positive

True Positive (TP) : Correctly predicts (Actual=0 the model predicts as 0)

True Negative (TN) : Correctly predicts (Actual=1 the model predicts as 1)

False Positive (FP) : Incorrectly predicts (Actual=0 the model predicts as 1)

False Negative (FN) : Incorrectly predicts (Actual=1 the model predicts as 0)

- **The sensitivity (*SENS*)** is the rate of TP over all of class 0. It can be defined as follows:

$$SENS = \frac{TP}{TP + FN}$$

- **The specificity (*SPEC*)** is the rate of TN over all of class 1. It can be defined as follows:

$$SPEC = \frac{TN}{TN+FP}$$

- **The precision** (***PRE***) is the rate of TP over all the positive events. It can be defined as follows:

$$PRE = \frac{TP}{TP+FP}$$

Due to the imbalanced-data. The data that belongs to each class is not equal and the performance measure is different from the binary classification.

- **Weighted Average Precision (PRE_{Avg}) is used as described:**

$$PRE_{Avg} = \frac{w_{i-1} \times PREC_{i-1} + w_i \times PREC_i}{w_{i-1} + w_i}$$

w_i represents the number of data points in each class where i is the number of classes.

5.2 Evaluation of 3D ACM from different parameter settings.

This experiment is done by selecting 6 important points related to the most distant point in the basal lobe and sharp curve at the basal and anterior of the lung. The superior and the posterior have no challenge point except the stop boundary condition. However, the anterior has another sharp edge which is not easy to detect in some specific cases that deviate from the normal conditions.

As mentioned in Chapter 4 Tab. 4.2, PARAM1 has the most error in the lower lobe at the bottom the error is 2.43 mm and 3.22 mm on average. Since the balloon force is sensitive to the external energy and the potential force to reach the boundary. It has a very high chance to exceed the boundary of the EI model. Therefore, the balloon force is controlled as a small number to prevent its sensitiveness. Moreover, the Gradient Vector Field (GVF) is the image energy that can help enhance the stopping boundary and also acts as the stop energy as well.

Table 5.2 Evaluation of 3D ACM from different parameter settings.

Parameter settings	Average displacement from the EE to EI (mm)											
	Top		Bottom		Front		Back		Left		Right	
	R	L	R	L	R	L	R	L	R	F	R	L
$PARAM_1$	0.1	0	2.43	3.22	0	0	0	0	0.64	0	0	0.48
$PARAM_2$	0	0	1.56	1.28	0.02	0.04	0	0	0.40	0	0	0.36
$PARAM_3$	0	0	0.84	0.52	0.03	0.04	0	0	0.42	0	0	0.44

1 pixel (X) = 0.2645833333 mm

5.3 Evaluation of lung lobe degree of rotation

This experiment is to detect the degree of rotation of the oblique and horizontal fissures as shown in Table 5.3. The LOF and ROF are approximately 45 degrees rotated with respect to the Z-axis and RHF is approximately 90 degrees with respect to the Z-axis. The Standard Deviation (SD) is high in Obstructive diseases for the LOF and ROF. This implies that the small airway disease may limit the airflow into some area in the EI model. The degree of rotation can help to interpret and understand the motion pattern of obstructive lung disease and overlapped diseases.

Table 5.3 Degree of rotation for each lung lobe with respect to Z-axis.

	Left Lung	**Right Lung**	
	Left Oblique Fissure	**Right Horizontal Fissure**	**Right Oblique Fissure**
Normal	44.3° (+/- 2.32)	87.5° (+/- 3.76)	43.1° (+/- 2.56)
Obstructive	48.0° (+/- 8.22)	91.3° (+/- 4.29)	44.3 (+/- 5.92)
Restrictive	43.2° (+/- 4.32)	79.4° (+/- 2.44)	46.2(+/- 3.12)

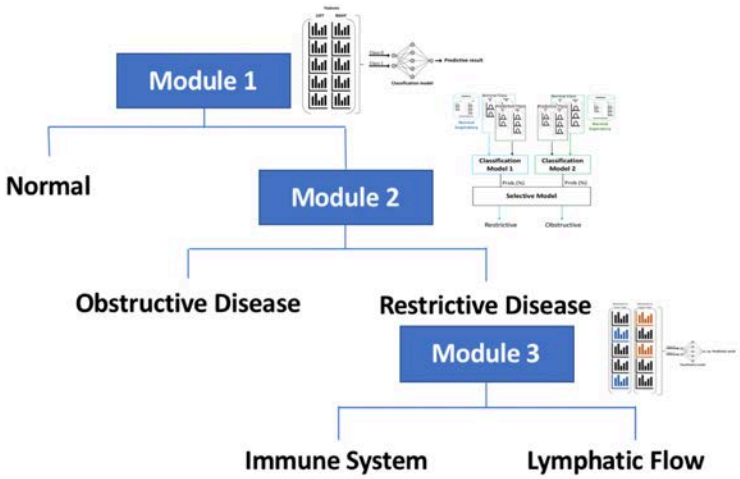

Fig. 5.1 the hierarchy predictive model.

5.4 Evaluation of Module 1: Classify normal and abnormal lungs.

The first module is to classify normal and abnormal lungs. Although the data set of a normal class is not high, it is useful to extract and learn the normal motion pattern to the predictive system. This can help avoid false positive detection. Even the false positive is not the serious condition but it can improve the efficiency of the overall system and screen the normal case out of the deviation from normal class. Tab. 5.4 shows the classification result of normal and abnormal. The total number of datasets is 100: normal 10 cases and abnormal 90 cases. The precisions of each class (PRE_0 and PRE_1) are calculated: PRE_0 is 50% for normal class and PRE_1 is 98.78% abnormal class. Then the weighted average precision (PRE_{AVG}) is shown at 93.20% on Table 5.4.

Table 5.4 Evaluation results of Module 1: Classify normal and abnormal lungs.

Module 1		**Actual Class**		**Evaluation**		
		normal	abnormal	PRE_0	PRE_1	PRE_{AVG}
Predict Class	normal	9	9	50.0%	98.78%	93.90%
	abnormal	1	81			

5.5 Evaluation of Module 2: classification of obstructive and restrictive lung diseases.

This module uses the pathological knowledge of the restrictive and obstructive lung diseases to classify. The restrictive lung disease is when the patient cannot take a full and deep inhalation. Therefore, when compared to the normal size of the lung in EI CT images, the patient with restrictive lung disease can be differentiated from the normal patient. In obstructive lung disease, the patient has a problem with exhalation. They cannot exhale naturally because there is some blocked area in the small airway or bronchus. To classify obstructive lung diseases, the EE CT images of the normal patient and obstructive lung disease patients are analyzed. The total numbers of dataset for this module are 90 cases: obstructive lung disease (Obs.) 48 sets and restrictive lung disease 42 sets. The precision of obstructive class (PRE_{Obs}) is 90.0% and the precision of restrictive class (PRE_{Res}) is 92.5%. The weighted average precision (PRE_{AVG}) is 91.06% as shown below on Table 5.5.

Table 5.5 Evaluation results of Module 2: Classify obstructive and restrictive diseases.

Module 2		**Actual Class**		**Evaluation**		
		Obs.	Res.	PRE_{Obs}	PRE_{Res}	PRE_{AVG}
Predict Class	Obs.	45	5	90.0%	92.5%	91.06%
	Res.	3	37			

5.6 Evaluation of Module 3: the classification of immune system and lymphatic system

This module is to detect the inhomogeneous motion pattern based on the causes of diseases, immune system and lymphatic system, which are also related to the expanding motion of each particular lobe. For the restrictive lung disease, the cause of disease is the interstitium which is the tissue and space around the pulmonary alveoli called alveolar capillary membrane. The dataset of this module is 42 sets: 19 sets for lymphatic system and 23 sets for the immune system. The precision of the lymphatic system (PRE_{Lym}) is 83.0% and the precision of the immune system (PRE_{Imm}) is 83.0%. Then, the weighted average precision of this module is 83.0% as shown on Table 5.6.

Table 5.6 Evaluation results of Module 1: Classify immune and lymphatic system.

Module 3		**Actual Class**		**Evaluation**		
		Imm.	Lym.	PRE_{Imm}	PRE_{Lym}	PRE_{AVG}
Predict Class	Imm.	15	3	83.33%	83.33%	83.33%
	Lym.	4	20			

To summarize the overall system, Fig. 5.2 compares the precision on each class from 3 modules. The highest performance is class 2 on module 1 which is to classify the normal to abnormal class. The third module is difficult to classify because of the variety of severity on the lung. The average precision on class 5 and class 6 is 83.33%. Fig. 5.3 shows the comparison among 3 classification. Again, the third module has more challenge to classify 2 different courses of restrictive lung disease.

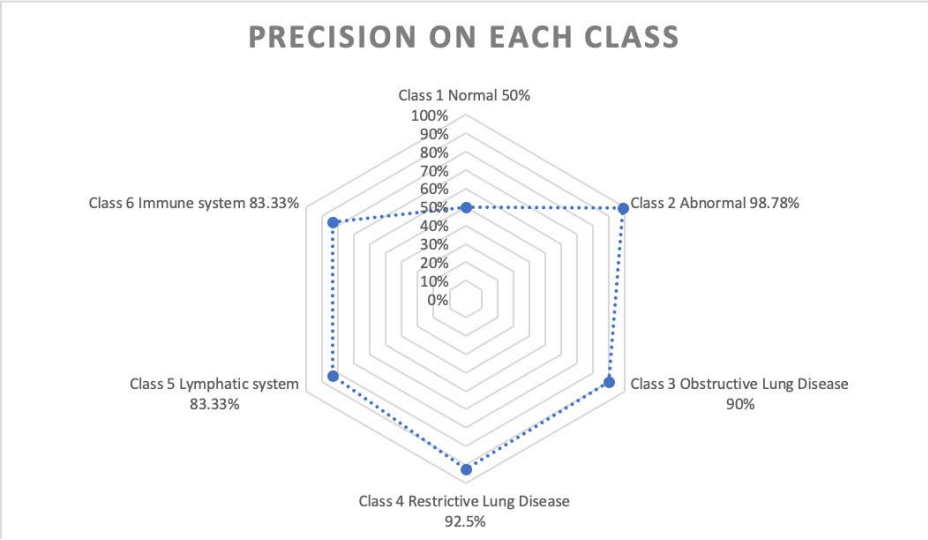

Fig. 5.2 The precision of each class: Class 1 is normal, Class 2 is abnormal, Class 3 is obstructive lung disease, Class 4 is restrictive lung disease, Class 5 is lymphatic system, and Class 6 is immune system.

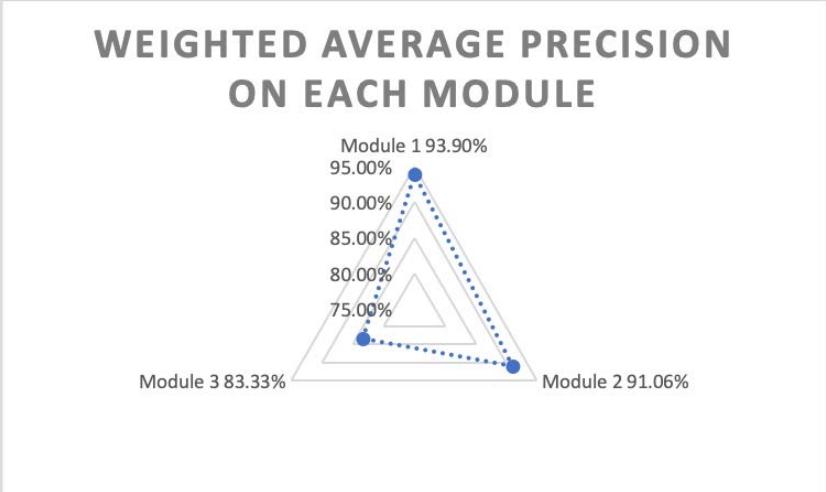

Fig. 5.3 The weighted average precision of 3 predictive modules.

Table 5.7 The evaluation of predictive model (Module 1-3)

Predictive Model		**Actual Class**		**Evaluation results**		
		Abnormal (0)	Normal (1)	PRE_0	PRE_1	PRE_{AVG}
Predict Class	Abnormal (0)	81	1	98.78	50.00%	93.90%
	Normal (1)	9	9			
	Obs. (0)	45	5	90.00%	92.50%	91.06%
	Res. (1)	3	37			
	Imm. (0)	15	3	83.33%	83.33%	83.33%
	Lym. (1)	4	10			

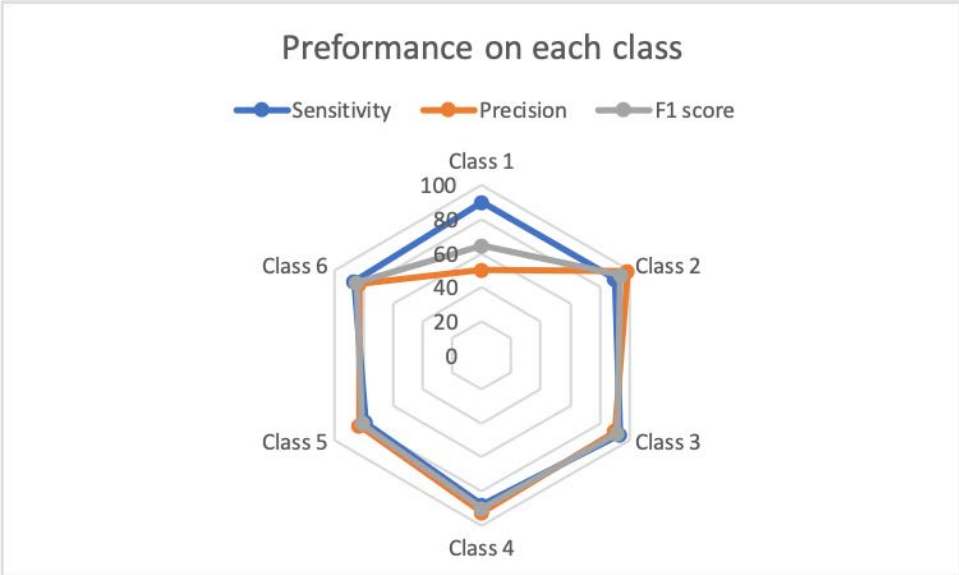

Figure 5.4 Compare the performance of each class by PRE, SENS, and F1 score

Fig. 5.4 shows the comparison of other measurement metrics which is SENS and F1 score. It is shown that the result of class 1 is varied based on the measurement metric such as PRE = 50.0%, SENS = 90%, and F1 score = 64.28%. Finally, the False Positive and False Negative is the important metric that needed to be considered. In the future work, the unbalanced data will be resampled in order to avoid this bias.

Chapter 6

Conclusion

6.1 Conclusion

This research introduces the new approach of the 3D active contour model to evaluate the velocity vectors of the lung motion and learning the inhomogeneous motion pattern from each lung lobe to generate the predictive model from the characteristic of breathing motion. The non-rigid registration model by using its biophysical model is applied. The velocity vectors between EI and EE models are evaluated by the corresponding points on the parametric surface model of the EE model to the EI model. The external energy from the EI models is the external force that pushes the 3D parametric surface reaching the boundary. The external forces such as balloon force and Gradient Vector Flow (GVF) were adjusted adaptively based on the Z_{ratio} which calculated from the ratio of the maximum value of EI to the EE model in Z-axis. Next, the feature representation is studied and evaluated based on the lung structure which is separated into 5 lobes. To screening the lung diseases into the normal, obstructive lung, and restrictive lung, the stepwise regression, and Artificial Neural Network technique are used to evaluate the result shown in Tab. 6.1.

The inhomogeneous motion pattern of lungs integrated with the medical-based knowledge can be used to analyze the lung diseases: **Module 1** by differentiating normal and inhomogeneous with motion patterns with PRE_{AVG}=93.90%, **Module 2** by separating restrictive and obstructive lung diseases with 90% of $PRE_{Obs.}$ And 92.5% of $PRE_{Res.}$, that makes the PRE_{AVG} is 91.06% dependent on the weight of each class. **Module 3** by basing on the cause and location of the disease which is the function of the immune and lymphatic system, the $PRE_{Imm.}$ = 83.33% and $PRE_{Lym.}$= 83.33% too and the final PRE_{AVG} = 83.33%. The false detection comes from the severity of the disease. When it is in the early stage, the change in motion is not too different compared to the healthy one. The solution on this limitation is to relabel and separate the subclass based on level of severity or to increase the size of data set in order to detect more the

pattern of lung motion. In this way, we may discover the new pattern of the motion. Lastly, the hierarchy predictive model in this research can be used for screening the lung diseases especially for the first and the second hierarchy to classify normal and abnormal class and obstructive and restrictive class.

6.2 Future works

- Reduce the false detection by finding more relative points between EE and EI inhomogeneous motion and studying more in feature representation and feature selection.
- Increase the number of database in order to discovery more motion patterns to analyze the lung diseases.
- Integrate more knowledge of pathology, radiology, and image processing to find the insight from the pattern of data.
- Improve the accuracy of the model to widely use for screening lung diseases.
- Develop the user friendly user interface (GUI)

6.3 Recommendations

Please see Appendix A

Appendix A

Comments from Committee Members

Q.1 On the presentation slide, the number of Abnormal is 90 in Table 7 but 80 patients appear in Table 8. Which is correct?

- (Assoc. Prof. Toshiaki Kondo)

There is a typo error on Table 8. The number of abnormal patients is 90. Table 1 shows the data sets on each class.

Table 1: The data sets on each class.

Class	Description	Data sets
Class 1	Normal	10
Class 2	Abnormal	90
Class 3	Obstructive Lung Disease	48
Class 4	Restrictive Lung Disease	42
Class 5	Lymphatic system	19
Class 6	Immune system	23

Q.2 The weighted average should be between the two values; higher and lower ones. There is something wrong in Tables 8 and 9 (on the presentation slide slide). The average cannot be lower than a smaller value and larger than a large value. If you think your results are correct, explain why.

- (Assoc. Prof. Toshiaki Kondo)

Ans: As mentioned in Question 1, there is a typo error at the weight parameter according to the number of data sets. Therefore, the weighted average result is 91.06% between the 2 values 92.5% with 48 patients and PRE_{Res} is 90% with 42 patients.

Q.3 In conclusion, PREabnormal is missing. Why don't you use a hexagon graph instead of a pentagon graph? PREobt is also wrong in the graph. Compare with Table 8.

- (Assoc. Prof. Toshiaki Kondo)

Ans: It can be shown by using hexagon graph. Fig. 1 shows the updated version of hexagon graph and Fig. 2 shows the weighted average precision on each predictive module.

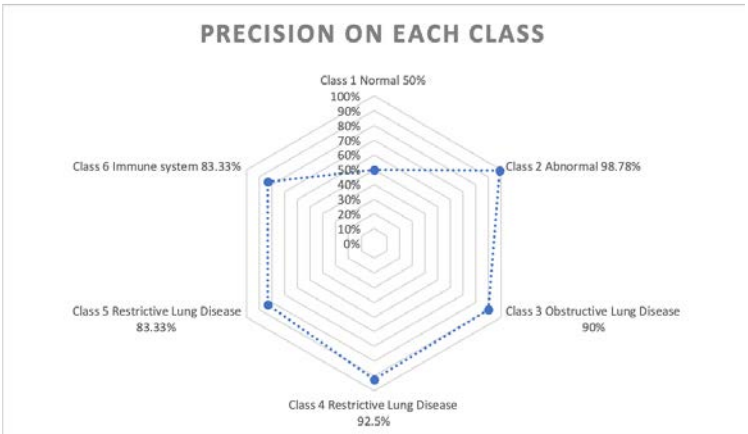

Figure 1. Precision on each class using Neural Network technique

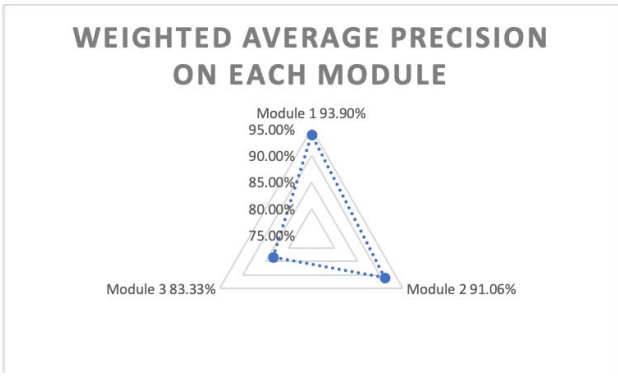

Figure 2. Weighted average precision on each class

Q.4 Why and how to evaluate the hierarchy predictive model?

- (Prof. Jianwu Dang)

Ans: We would like to evaluate the accumulative accuracy of the system by using the hierarchy predictive model as shown in Fig.3. The output of the higher level effects the input dataset of the lower level (Module 1 - 3). Therefore, we need to use this model to evaluate the model performance.

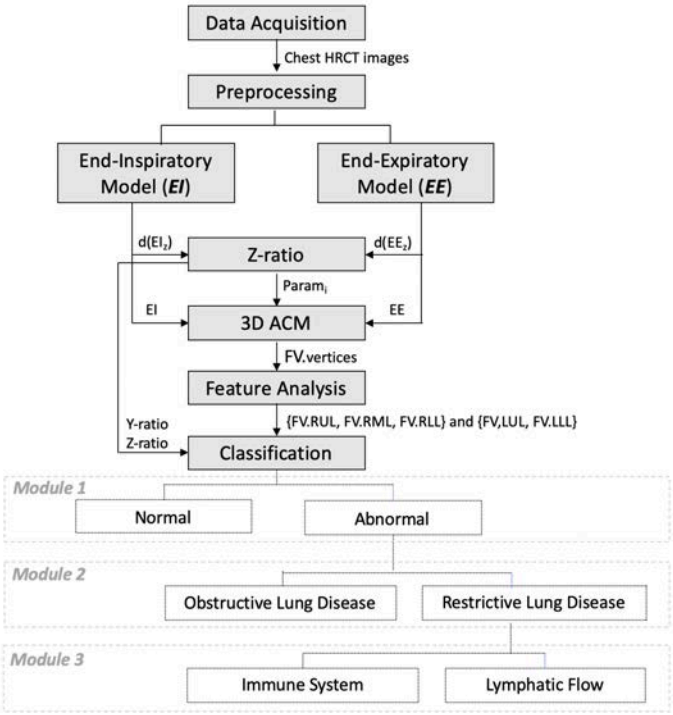

Figure 3.the overview of the purposed technique and the hierarchy predictive model.

Q.5 It is velocity vector or displacement?

- (Prof. Jianwu Dang)

Ans: For the velocity vector map, the expanding lung motion is estimated from the end-expiratory (EE) to the end-inspiratory (EI). The motion is considered as a vector and it contains magnitude and orientation. However, this research focuses on the magnitude by using the function as shown below:

$$\boldsymbol{d(x', y', z': x, y, z) = \sqrt{(x' - x)^2 + (y' - y)^2 + (z' - z)^2}}$$

Generally, the first criteria for clinical screening to diagnose obstructive and restrictive lung diseases is defined by the Pulmonary Function Tests (PFTs). The volume of lungs and ability to expanding and shrinking is considered to classify the type of lung diseases.

The PFTs consists of three main parameters:

1). The Forced Vital Capacity (FVC) test shows the amount of air that a person can quickly and forcefully breathe out, after a deep breath,

2). the Forced Expiratory Volume in One Second (FEV1) test shows the amount of air a person can forcefully exhale in one second of the FVC test, and

3). the Total Lung Capacity (TLC) test describes the volume of air remaining in the lung after exhalation.

The FEV1/FVC ratio is used to diagnose the type of lung disease and the severity of a disease. The FEV1/FVC ratio is decreased in the obstructive pattern and increased in the restrictive pattern.

For example, an FEV1/FVC ratio of less than 0.7 [1] is considered as COPD and the stage of COPD is classified by the percent of FEV1: Mild FEV1 $\geq$ 80%,

Moderate 50%≦FEV1<80%, Severe 30% ≦ FEV1< 50%, and Very Severe FEV1< 30%. These tests are the gold standard to diagnose COPD [2,3]. The TLC is increased or normal in an obstructive pattern by the remaining air in the lungs and decreased in a restrictive pattern.

[1] P. P. Walker, P. Mitchell, F. Diamantea, C.J. Warburton, and L. Davies, "Effect of primary-care spirometer on the diagnosis and management COPD", European Respiratory Journal 2006, Vol. 28: 945-952. DOI:10.1183/09031936.00.00019306

[2] Y. Qu, Y. Cao, M. Liao, and Z. Lu, "Sagittal-Lung CT Measurements in the Evaluation of Asthma-COPD Overlap Syndrome: A Distinctive Phenotype from COPD alone", Radio Med (2017) 122:487-497. DOI: 10.1007/s11547-017-0743-9

[3] R. A. Hartley, B. L. Barker, C. Newby, M. Pakkal, S. Baldi, R. Kajekar, R. Kay, M. Laurencin, R P. Marshall, A. R. Sousa, H. Parmar, S. Siddiqui, S. Gupta, and C. E. Brightling, "Relationship between Lung Function and Quantitative Computed Tomographic Parameters of Airway Remodeling, Air Trapping, and Emphysema in Patients with Asthma and Chronic Obstructive Pulmonary Disease: A Single-Center Study", vol. 137, no. 5, (2016) DOI: 10.1016/j.jaci.2016.02.001

Q.6 Evaluation of accuracy of 3D ACM from adaptive parameter settings, if this number of errors is reduced, can it help to improve the accuracy of ACM in the next step.

– (Assoc. Prof. Shinobu Hasegawa)

Ans:

There is a challenge point of ACM on the sharp corner. In the case of sharp corner, we need to increase the balloon force and also the Gradient Vector Flow (GVF) in order to push the parametric contour to the boundary of EI model. We cannot apply the same parameter to all datasets because it shows the difference characteristics to expanding as shown in Fig. 5. Therefore, the diameter of 3D model is evaluated called Z_{ratio}. The Z_{ratio} is introduced to distinguish the different sets of shape estimated by the ratio of diameter EI to EE on the Z-axis as shown in Z_{ratio} equation.

$$\boldsymbol{Z_{ratio} = \frac{|\max(EI.z) - \min(EI.z)|}{|\max(EE.z) - \min(EE.z)|}}$$

Where $|\max(EI.z) - \min(EI.z)|$ represents the diameter in Z direction of EI model and $|\max(EE.z) - \min(EE.z)|$ is the diameter in Z direction of EE model.

By using Z_{ratio}, it can overcome the difficulty of the parametric contour to control the The shape and size of lung is separated in to 3 sets based on the data set of this study and then the weighted parameters are assigned each set called $PARAM_1$, $PARAM_2$, and $PARAM_3$ as shown in Fig.4. When the Z_{ratio} is higher than 1.2, $PARAM_1$ is applied, the challenge of $PARAM_1$ is the sharp edge in the lower lung, the balloon force and GVF are tuned. $PARAM_2$ represents the normal or slightly abnormal lungs where Z_{ratio} is between 1 to 1.2. $PARAM_3$ is the abnormality cases where mostly appears in patient with air trapping problem (obstructive lung disease).

If we can reduce the error from 3D ACM technique by using adaptive parameters, it will help improve the accuracy for in the classification model too.

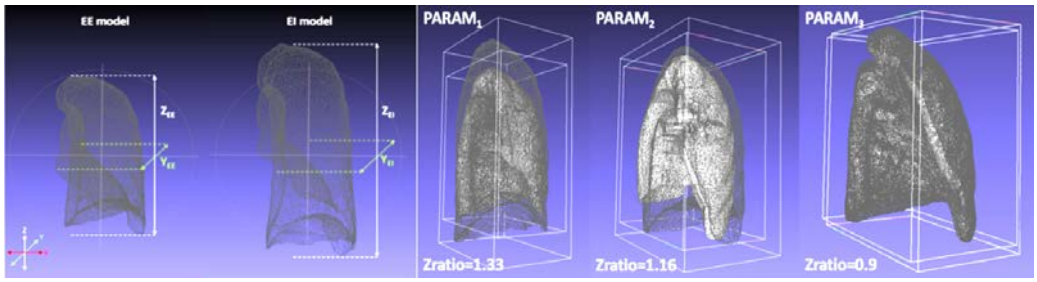

Figure 4. $\boldsymbol{Z_{ratio}}$ estimation from EI and EE models and examples of a dataset with 3 different parameter function: $\boldsymbol{PARAM_1}$, $\boldsymbol{PARAM_2}$, and $\boldsymbol{PARAM_3}$

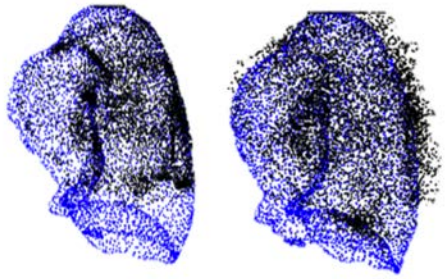

Figure 5. Examples when the magnitudes of weighted parameters are unbalanced.

Q.7 Unbalanced data problem and how to fix it? Example: sampling data

– (Assoc. Prof. Shinobu Hasegawa)

Ans: To solve the unbalanced data problem, we can resample the data by copying the minority class which is 10 datasets. However, there are the criteria to identify the normal lung and also the factor that affects lung volume such as age, height, people who live at higher/lower altitudes. In particular FEV1/FVC (as mentioned in Question 5) is used to distinguish the obstructive and restrictive lung diseases. For the restrictive lung disease, the volume is decreased and for the obstructive lung disease, there is the air trapped inside, then flow rates are impeded.

Therefore, to resampling the normal lungs we need to consider the physical environmental factors and selected the one that represents the main characteristics of the healthy lung.

However, if the number of data set is not so much difference we can use F1 score or average precision to evaluate the classification model by using the number of instances of each class. We also need to specify the considering points

Q.8 Why we need to consider the normal case. Normally the data from the hospital is mostly unhealthy. Why we need to separate the normal and abnormal according to the first Module.

– (Assoc. Prof. Shinobu Hasegawa)

Ans. To classify the normal from the abnormal cases, it can help avoid the false positive (FP) from the patient who has no lung disease. However, the medical doctor concerns the accuracy of false negative (FN) more than the false positive (FP). If our focus group is the lung disease classification, we can use module 2 and 3 to classify. However, for the overall system in practical, it might have the false positive case to the screening system. Therefore, the module 1 is still important to learn and classify the false positive case.

Q.9 Normally ACM is used to segmentation object and in this research, ACM is used to estimate the motion?

- (Prof. Mineo Kaneko)

Ans.

The 3D ACMs are generally used as a non-rigid segmentation-based technique, especially in biomedical images. The concept of 3D ACM is to minimize the internal and external energies, and the final evaluation of the active contour will be stopped by the desired boundary of the target.

The 3D Parametric Active Contour Model is performed to estimate the velocity vector between the EE and EI lung models. A mesh represents the control points of the 3D active contour. The energy function in 3D ACM develops the parameter function to control the control points in more dimensions as $\boldsymbol{v} : [\mathbf{0}, \mathbf{1}] \times [\mathbf{0}, \mathbf{1}] \rightarrow \mathbb{R}^{\mathbf{3}}$. The 3D contour is described by a function of *v*. The contour is placed on an image as $\boldsymbol{f} : \mathbb{R}^{\mathbf{3}} \rightarrow \mathbb{R}$. The snake model combines the internal energy $\boldsymbol{E_{int}}$ and external energy

$\boldsymbol{E_{ext}}$into $\boldsymbol{E = E_{int}(v) + E_{ext}(v)}$. The 3D image force concerns the movement in 3 directions of the parametric curve in $\boldsymbol{E_{int}(v)}$. Therefore, the parameter function ($\boldsymbol{v = v(s,r) = [X(s,r), Y[s,r], Z(s,r)]}$) is added to control the corresponding points (or the control points) where $\boldsymbol{X, Y, Z}$ are the corresponding coordinate function of the surface.

The internal energy $\boldsymbol{E_{int}(v)}$ can be expressed as

$$\boldsymbol{E_{int} = \iint [\alpha_s |v'_s|^2 + \alpha_r |v'_r|^2] + [\beta_s |v''_{ss}|^2 + \beta_r |v''_{rr}|^2 + \beta_{sr} |v''_{sr}|^2] \, dsdr}$$

where $\boldsymbol{\alpha_s}$ and $\boldsymbol{\alpha_r}$ denote the elasticity, respectively, $\boldsymbol{\beta_s}$ and $\boldsymbol{\beta_r}$ are the corresponding rigidities, and $\boldsymbol{\beta_{sr}}$ is the resistance to twist.

The external energy $\boldsymbol{E_{ext}(v)}$ is the image force of the boundary.

In this work, the EI model is modified from the 3D surface (EI model) to 3D matrix of contour point by setting the boundary of $\boldsymbol{I_{EI}(x, y, z) = 1}$ and the inner and outer of a closed parametric surface (EE model) are set as 0. The $\boldsymbol{E_{ext}(v)}$ represents by $\boldsymbol{E_{image}(v)}$. $\boldsymbol{E_{image}(v)}$ shows the features of the EI model such as the boundary and represented it by potential force fields or the gradient of the image $\boldsymbol{\nabla p(v, f)}$ under the closed plane conditions. Next, the energy ($\boldsymbol{E = E_{int}(v) + E_{ext}(v)}$) is minimized by using the Euler-Lagrange equation to find the *v* that satisfies the equation balances the internal force and image force. When all energies are balanced, the total energy is minimum as shown.

$$\boldsymbol{[\alpha_s |v'_s|^2 + \alpha_r |v'_r|^2] - [\beta_s |v''_{ss}|^2 + \beta_r |v''_{rr}|^2 + \beta_{sr} |v''_{sr}|^2] = -\nabla p(v, f)}$$

Therefore, the corresponding point on the parametric surface from EE to EI model can be used to evaluate the expanding motion of lungs.

Q.10 Why select Neural Network technique as a classification technique, how about the Support Vector Machine (SVM)? Comparing to the previous work, SVM is better than Neural Network, why you select NN?

– (Assoc. Prof. Waree Kongprawechnon)

Ans.

Now the SVM is used to compare the accuracy to the neural network technique. Due to the size of training data, using SVM can provide the maximum margin between 2 classes by using RBF kernel function. For the estimation model, we still use the hierarchy predictive model to evaluate the performance of the model because SVM has a limitation to binary classification.

Q.11 The time consuming of Finite Element Method is under the same assumption as the proposed technique?

– (Assoc. Prof. Waree Kongprawechnon)

Ans.

For the time consuming, there are 3 factors that highly affect which are the number of elements, the number of iterations and preprocessing method. If those factors are complicated, it will take more time consuming. For the Finite Element Method (FEM), The preprocessing of FEM is started by setting the geometric construction, discretization, shape function, element equation, initial condition, and then material properties. The mesh convergence is also analyzed be selected the suitable number of mesh. In the biomedical image, the elements of mesh are approximately 10,000 to 20,000 elements. The number of elements and conditions (by shape and delicacy of 3D mesh) will affect the time consuming for tuning FE simulation which may use 13 hours [4] or 86 hours [5]. Some research solves this problem by considering the

landmark points which can reduce the computed elements to 300 – 400 elements [6-7].

However, this research using 3D mesh for the initialization by assigning it to the initial parametric curve of the 3D ACM which is also generated from 3D mesh. The alignment for registration and the parameter setting is applied before the iteration process starts. The adaptive parameter is calculated by size of the lung in order to adjust the controlled energy of both internal energy such as the tension and rigidity of the parametric curve and external energy such as balloon force and gradient vector flow. The adaptive parameter can also help to reduce the simulation time by using the set of parameters based on the physical shape of lungs. In this research, the approximate time-consuming starting from 3D mesh to the last iteration is about 10 minutes per model.

[4] L. Han, H. Dong, J. R. McClelland, L Han, D. J. Hawkes, and D. C. Barratt, A hybrid patient-specific biomechanical model-based image registration method for the motion estimation of lungs, Medical Image Analysis, Vol. 29, pp. 87-100 (2017)

[5] M. Zehtabian, R. Faghihi, M. A. Mosleh-Shirazi, A. R. Shakibafard, M. Mohammadi, and M. Baradaran-Ghahfarokhi, "A Fast Model for Prediction of Respiratory Lung Motion for Image-Guided Radiotherapy: A Feasibility Study", Iran. J. Radiat. Res., Vol. 10(2), pp. 73-81 (2012)

[6] X. Liu, R. R. Saboo, and S. M. Pizer, A shape-navigated image deformation model for 4D lung respiratory motion estimation, IEEE ISBI (2009)

[7] P. A. Yushkevich, J. Piven, H. C. Hazlett, R. G. Smith, S. Ho, J. C. Gee, and G. Gerig, User-guided 3D active contour segmentation of anatomical structures: significantly improved efficiency and reliability, NeuroImage, pp. 1116-1128 (2006)

Publications

International Journals

Pikul Vejjanugraha, Kazunori Kotani, Waree Kongprawechnona, Toshiaki Kondo, Kanokvate Tungpimolrut (2020) A Screening Technique for Analyzing Interstitial Lung Disease using Texture and Pattern analysis from CT images in the Coronal Plane, Journal of Intelligent Informatics and Smart Technology **[Accepted]**

Pikul Vejjanugraha, Kazunori Kotani, Waree Kongprawechnona, Toshiaki Kondo, Kanokvate Tungpimolrut (2020). An Automatic Diagnosis of Lung Diseases by Analyzing an Inhomogeneous Motion on 3D Shape of Lung CT Images, Walailak Journal of Science and Technology (WJST) **[Under Review]**

Pikul Vejjanugraha, Waree Kongprawechnona, Toshiaki Kondo, Kanokvate Tungpimolrut, Kazunori Kotani (2017). An Automatic Screening Method for Primary Open-angle Glaucoma Assessment using Binary and Multi-class Support Vector Machines. ScienceAsia 43, 229-239 doi:10.2306/scienceasia1513- 1874.2017.43.229 **[Published]**

National Conference

P. Vejjanugraha, K. Kotani, W. Kongprawechnon, T. Kondo, K. Tungpimolrut (2015) An Automatic Screening Technique for Glaucoma in High-Myopic Eyes by Detecting the Morphologic Changes of the Optic Disc (OD) and Beta-Parapapillary Atrophy (β-PPA). Image Media Processing Symposium, pp.52-53

International Conferences

P. Vejjanugraha, M. Kanazashi, J. Izawa., K. Kotani, W. Kongprawechnon (2016) Inhomogeneous Motion Analysis of 3-D Lung Surface by Evaluating Feature Correspondence of Active Surface Model", SICE Annual Conference 2016, September 20-23, 2016, Tsukuba International Congress Center, Tsukuba, Japan (2016)

P. Vejjanugraha, K. Kotani, W. Kongprawechnon, T. Kondo, K. Tungpimolrut. (2018) A Quantification Technique of Air Trapping in Lungs using Stepwise Regression and Neural Network from End-inspiratory and End-Expiratory CT-images, 13th International Conference on Knowledge, Information and Creativity Support Systems, November 15-17, 2018. Pattaya, Thailand.

References

[1] T. Hashimoto, C. Wang, and J. Masumoto, *Quantification of the respiratory activity of the lung using CT Images*, FUJIFILM Research and development, No. 60-2015 (2015)

[2] A. O. D. C. Filho, A.C.Silva, A. C. D. Paiva, and R. A. Nunes, and M. Gattass, *3D shape analysis to reduce false positives for lung nodule detection system*, Med Biol Eng Conput (2017), 55: 1199-1213

[3] C. J. Galban, M. K. Han, J. L. Bose, Computed tomography-based biomarker provides uniques signature for diagnosis of COPD phenotypes and disease progression, Nature Medicine, Vol. 18, No. 11, (2012)

[4] Z. Tatjana and S. Busayarat, *Computer-aided analysis and interpretation of HRCT images of the lung, Chapter Theory and Applications of CT imaging and Analysis*, (2011)

[5] Ruth A. Hartley, *Relationship between lung function and quantitative computed tomographic parameters of airway remodeling, air trapping, and emphysema in patients with asthma and chronic obstructive pulmonary disease: A single-center study*, vol. 137, no. 5, (2016)

[6] H. K. Reddel, *Treatment of overlapping asthma-chronic obstructive pulmonary disease: Can guildlines contributed in an evidence-free zone?,* vol. 136, No. 3 (2015)

[7] P. P. R. Filho, P. C. Cortez, *Novel and powerful 3D adaptive cripes active contour method applied in the segmentation of CT lung images*, Medical Image analysis Vol. 35, pp. 503-516 (2017)

[8] C. P. Hersh, G. R. Washko, R. S. J. Estepar, *Paired inspiratory-expiratory chest CT scans to assess for small airways disease in COPD*, Respiratory Research (2013), pp. 14-42.

[9] Y. Qu, Y. Cao, M. Liao, and Z. Lu, *Sagittal-lung CT measurements in the evaluation of asthma-COPD overlap syndrome: a distinctive phenotype from COPD alone*, Radiol Med (2017), Vol. 122, pp. 487-494.

[10] R. Mukundan, *Reconstruction of high resolution 3D meshes of lung geometry from HRCT contours*, IEEE International Symposium on Multimedia (2016)

[11] H. Watz, B. Waschki, and T. Meyer, *Decreasing cardiac chamber sizes and associated heart dysfunction in COPD*, American College of Chest Physicians, (2010)

[12] N. H. Johari, J. Balaiyah, and Z. Ahmed, *Effect of chronic obstructive pulmonary disease on airflow motion using computational fluid dynamics analysis*, IEEE 2014 International Conference on Computer, Communication, and Control Technology (2014)

[13] X. Liu, R. R. Saboo, and S. M. Pizer, *A shape-navigated image deformation model for 4D lung respiratory motion estimation*, IEEE ISBI (2009)

[14] A. Bhavsar, G. Wu, and D. Shen, *Motion-guided resolution enhancement for lung 4D-CT*, 13th International Conference on Control, Automotive, Robotics and Vision (2014)

[15] M. Zehtabian, R. Faghihi, M.A. Mosleh-Shirazi, A.R. Shakibafard, M. Mohammadi, M. Baradaran-Ghahfarokhi, A fast model for prediction of respiratory lung motion for image-guided radiotheraphy: A feasibility study, Iran. J. Radiat. Res., Vol. 10(2), pp. 73-81 (2012)

[16] L. Han, H. Dong, J. R. McClelland, L Han, D. J. Hawkes, and D. C. Barratt, A hybrid patient-specific biomechanical model based image registration method for the motion estimation of lungs, Medical Image Analysis, Vol. 29, pp. 87-100 (2017)

[17] P. A. Yushkevich, J. Piven, H. C. Hazlett, R. G. Smith, S. Ho, J. C. Gee, and G. Gerig, User-guided 3D active contour segmentation of anatomical structures: significantly improved efficiency and reliability, NeuroImage, pp. 1116-1128 (2006)

[18] G. K. L. Tam, Z-Q. Cheng, Y-K. Lai, F. C. Langbein, *Registration of 3D point clouds and meshes: a survey from rigid to non-rigid*, Vol. 6, No.1 (2007)

[19] P. P. R. Filho, P. C. Cortez, A. C. D. S. Barros, *Novel adaptive balloon active contour method based on internal force for image segmentation-A systematic evaluation on synthetic and real images*, International Journal, Expert systems with applications (2014)

[20] S. Ukil and J. M. Reinhardt, *Anatomy-guided lung lobe segmentation in X-ray CT image*s, IEEE Transaction on Medical Imaging. Vol. 28, No.2 (2009)

[21] Q. Wei, Y. Hu, G. Gelfand, and John H. MacGregor, *Segmentation of Lung Lobes in High-Resolution Isotropic CT Images, IEEE Transactions on biomedical engineering*, Vol. 56, No. 5, (2009)

[22] Q. Wei, Y. Hu, *A Hybrid approach to segmentation of diseases lung lobes*, IEEE Journal of Biomedical and Health Informatics, Vol. 18, No.3 (2014)

[23] S. Qi, H. J. W. V. Triest, Y. Yue, M. Xu, and Y. Kang, Automatic pulmonary fissure detection and lobe segmentation in CT chest images, BioMedical Engineering OnLine, pp. 13-59 (2014)

[24] M.J.Fuller, The Fissures of the Lung, source: Wright Radiology of the Chest and Related Conditions: Together with an Extensive Illustrative Collection of Radiographs CRC Press, 2002